HHS Public Access

Author manuscript

Nature. Author manuscript; available in PMC 2016 April 11.

Published in final edited form as:

Nature. 2015 February 12; 518(7538): 249–253. doi:10.1038/nature13923.

RNA helicase DDX21 coordinates transcription and ribosomal RNA processing

Eliezer Calo[1,*], **Ryan A. Flynn**[2,*], **Lance Martin**[2], **Robert C. Spitale**[2], **Howard Y. Chang**[2], and **Joanna Wysocka**[1,3]

[1]Department of Chemical and Systems Biology, Stanford University School of Medicine, Stanford, California 94305, USA

[2]Howard Hughes Medical Institute and Program in Epithelial Biology, Stanford University School of Medicine, Stanford, California 94305, USA

[3]Department of Developmental Biology, Stanford University School of Medicine, Stanford, California 94305, USA

Abstract

DEAD-box RNA helicases are vital for the regulation of various aspects of the RNA life cycle[1], but the molecular underpinnings of their involvement, particularly in mammalian cells, remain poorly understood. Here we show that the DEAD-box RNA helicase DDX21 can sense the transcriptional status of both RNA polymerase (Pol) I and II to control multiple steps of ribosome biogenesis in human cells. We demonstrate that DDX21 widely associates with Pol I- and Pol II-transcribed genes and with diverse species of RNA, most prominently with non-coding RNAs involved in the formation of ribo-nucleoprotein complexes, including ribosomal RNA, small nucleolar RNAs (snoRNAs) and 7SK RNA. Although broad, these molecular interactions, both at the chromatin and RNA level, exhibit remarkable specificity for the regulation of ribosomal genes. In the nucleolus, DDX21 occupies the transcribed rDNA locus, directly contacts both rRNA and snoRNAs, and promotes rRNA transcription, processing and modification. In the nucleoplasm, DDX21 binds 7SK RNA and, as a component of the 7SK small nuclear ribonucleoprotein (snRNP) complex, is recruited to the promoters of Pol II-transcribed genes encoding ribosomal proteins and snoRNAs. Promoter-bound DDX21 facilitates the release of the positive transcription elongation factor b (P-TEFb) from the 7SK snRNP in a manner that is dependent on its helicase activity, thereby promoting transcription of its target genes. Our results uncover the multifaceted role of DDX21 in multiple steps of ribosome biogenesis, and provide evidence implicating a mammalian RNA helicase in RNA modification and Pol II elongation control.

Correspondence and requests for materials should be addressed to J.W. (wysocka@stanford.edu) or H.Y.C. (howchang@stanford.edu).

*These authors contributed equally to this work.

Author Contributions H.Y.C. and J.W. supervised the project; E.C. and R.A.F. conceived and designed the study; E.C. and R.A.F. performed experiments and analysed ChIP-seq data. R.A.F. performed iCLIP and L.M., R.C.S. and R.A.F. analysed iCLIP data; R.A.F., E.C., J.W. and H.Y.C. wrote the manuscript with input from all co-authors.

Author Information All sequencing data have been deposited in Gene Expression Omnibus (GEO) data repository under accession number GSE56802. Reprints and permissions information is available at www.nature.com/reprints.

The authors declare no competing financial interests. Readers are welcome to comment on the online version of the paper.

Supplementary Information is available in the online version of the paper.

RNA helicases are highly conserved enzymes that use the energy of ATP to remodel RNA secondary structures and ribonucleoprotein complexes[2,3] during various steps of RNA metabolism. In particular, the nucleolar helicase DDX21 is required for pre-rRNA processing[4,5], but the specific mechanism underlying this requirement remains unknown. Notably, DDX21 also influences c-Jun[6] transcriptional activities, suggesting a potential role in gene expression. To explore this, we first interrogated the chromatin association of DDX21 in HEK293 cells by chromatin immunoprecipitation followed by high-throughput DNA sequencing (ChIP-seq). Given that pre-rRNA processing occurs coordinately with rDNA transcription, we examined binding of DDX21 to the rDNA locus (Fig. 1a). DDX21 broadly, but specifically, associated with the transcribed region of the rDNA, but not with the intergenic spacer, a profile characteristic of known Pol I-associated co-transcriptional regulators[7,8]. In addition to rDNA binding, we identified 4,420 high-confidence peaks, most residing within 5 kilobases (kb) from annotated Pol II transcriptional start sites (Fig. 1b). DDX21-bound promoters had, on average, high enrichment of Pol II and active chromatin marks (histone H3 Lys 4 trimethylation (H3K4me3), H3K27 acetylation (H3K27ac) and H3K9ac), but were depleted for repressive (H3K27me3 and H3K9me3) and promoter-distal (H3K4me1) marks (Fig. 1c, d). Analysis of transcription factor motifs enriched at DDX21-bound regions uncovered recognition motifs of factors implicated in cell growth and proliferation (for example, E2F, STAT1, NRF1 and ETS; Extended Data Fig. 1a). ChIP-seq results were verified by ChIP-qPCR (quantitative PCR) in two additional human cell lines, with all interrogated target regions showing enrichment by qPCR (Extended Data Fig. 1b and data not shown), indicating that the chromatin interactions of DDX21 are reproducible across multiple cell types.

Gene Ontology analyses of DDX21-bound regions revealed specific and highly significant association with several regulatory arms of the ribosomal pathway (Fig. 1e). To verify this further, we compared annotations of DDX21-bound promoters to those H3K4me3-enriched but DDX21-unbound (Extended Data Fig. 1c). As expected, DDX21-bound promoters were enriched for ribosomal Gene Ontology terms, while DDX21-unbound promoters were enriched for other biological processes (Extended Data Fig. 1d). DDX21 binding was evident at promoters of genes encoding components of both the 40S (for example, *RPS3*) and 60S (*RPL23A* and *RPL8*) subunits (Fig. 1f). Messenger RNAs that encode ribosomal proteins often harbour snoRNAs in their introns[9]. DDX21 binds promoters of more than 80% of snoRNA-containing host genes; those unbound are poorly expressed in HEK293 cells (Fig. 1g and Extended Data Fig. 1e–g).

To examine the effect of DDX21 on transcription, we depleted the protein using two independent short interfering RNA (siRNA) pools (Fig. 1h and Extended Data Fig. 2a). *DDX21* knockdown decreased the steady-state levels of transcripts originating from DDX21-bound promoters, but had minimal effect on the unbound gene transcripts (Fig. 1h and Extended Data Fig. 2b). To explore whether DDX21 directly regulates transcription of ribosomal mRNAs, we measured the effect of DDX21 depletion on the synthesis of nascent transcripts upon release from the transcriptional elongation block induced by the kinase inhibitor flavopiridol[10,11]. We transfected HEK293 cells with control or *DDX21* 3′untranslated region (UTR) siRNAs, followed by expression of siRNA-resistant wild-type ($DDX21^{WT}$) or ATPase-defective[12] DDX21 (herein $DDX21^{SAT}$; Fig. 1i and Extended Data

Fig. 2c). *DDX21* knockdown impaired the production of nascent transcripts originating from DDX21-bound promoters, and this effect was rescued by the introduction of $DDX21^{WT}$, but not $DDX21^{SAT}$ (Fig. 1j and Extended Data Fig. 2d). Similar results were obtained on transcripts originating from the rDNA locus (Extended Data Fig. 2e). By contrast, non-target genes were minimally affected by the loss or ectopic expression of DDX21 (Fig. 1j and Extended Data Fig. 2d). Thus, DDX21 associates with and positively regulates transcription of Pol I- and Pol II-dependent ribosomal genes in a helicase-dependent manner.

The aforementioned observations prompted us to investigate potential crosstalk between DDX21 functions across nuclear compartments. Consistent with previous studies[13], inhibition of Pol I with either CX-5461 or a low dose of actinomycin-D (ref. 14) displaced DDX21 from the nucleolus, whereas localization of the nucleolar protein fibrillarin was not affected under these conditions (Fig. 2a and Extended Data Fig. 3a, b). Notably, hour-long inhibition of Pol II with flavopiridol recapitulated the nucleolar exclusion of DDX21 (Fig. 2a). By contrast, serum starvation or treatment with metabolic inhibitors impacting either cellular respiration or the mTOR pathway did not alter DDX21 localization (Extended Data Fig. 4), underscoring the preferential sensitivity of DDX21 to transcriptional inhibition. Furthermore, inhibition of either Pol I or II impaired the association of DDX21 with both the rDNA and Pol II-regulated promoters (Fig. 2c and Extended Data Fig. 3c, d). This change in chromatin association was not due to widespread chromatin silencing and compaction, as inhibitors did not affect CTCF binding at the rDNA- or Pol II-regulated chromatin (Extended Data Fig. 3e, f). Therefore, the chromatin association of DDX21 relies on the transcriptional status of either Pol I or II, suggesting coordination of the functions of DDX21 across subnuclear compartments.

The roles of DDX21 in transcription and rRNA processing are dependent on its intact helicase domain[4,6]. We proposed that defining the RNA interactome of DDX21 would reveal insights into the molecular mechanisms underlying its diverse functions. To identify DDX21-associated RNAs systematically, we performed tandem purification iCLIP (individual-nucleotide-resolution crosslinking and immunoprecipitation)[15] (Fig. 3a and Extended Data Fig. 5a, b) in HEK293 cells induced to express Flag- and haemagglutinin-tagged DDX21 (Flag–HA–DDX21). DDX21interacts with a diverse set of RNAs, of which rRNA and snoRNAs were most highly represented, while mRNAs contributed only 1.1% of the iCLIP reads (Fig. 3b). Gene ontology term and KEGG pathway analysis linked these mRNAs to ribosome function (Fig. 3b). Comparisons between DDX21 iCLIP targets and those of the splicing factor hnRNP-C[16] revealed little overlap, underscoring the specificity of our results (Extended Data Fig. 5c–e). We further confirmed select iCLIP interactions by ultraviolet RNA immunoprecipitation and quantitative reverse transcription PCR (qRT–PCR) (Extended Data Fig. 5f).

rRNA and snoRNAs represent candidate direct partners for DDX21-mediated rRNA processing function. DDX21 broadly crosslinks to rRNA, with the strongest binding overlapping 2′-*O*-methylation (2′-*O*me) and pseudouridylation (Ψ) sites (Fig. 3c), which are targeted and modified by snoRNP complexes[17]. Furthermore, DDX21 robustly interacts with regions in the 5′ external transcribed spacer, which is bound and processed by the U3 snoRNA[18]. Consistently, U3 is the most enriched short repetitive RNA of DDX21,

crosslinking to DDX21 in two distinct 5′ and 3′ regions of known rRNA targeting function[18] (Extended Data Figs 6f and 8c). iCLIP of DDX21^{SAT} revealed that it retained the ability to bind the major classes of RNA recovered with the wild-type enzyme (Extended Data Fig. 6a–d). However, there was a marked restriction of DDX21^{SAT} to 18S rRNA (Extended Data Fig. 6e). Notably, the inability of DDX21^{SAT} to bind the 5′external transcribed spacer was accompanied by the loss of the 5′ end binding to U3 (Extended Data Fig. 6f). Importantly, marked loss of DDX21^{SAT} association with the rRNA occurred in the absence of transcriptional defects in snoRNA production (Extended Data Fig. 6g).

Consistent with preferential association of DDX21^{WT} at rRNA modification sites, snoRNAs represent the principal class of DDX21-bound RNAs (Fig. 3d), as exemplified by snorD66 and snorA67, representing the C/D- and H/ACA-box subfamilies, respectively. DDX21 crosslinked most robustly outside the ‘box’ motifs (Extended Data Fig. 7a, b), a pattern distinct from canonical snoRNP-binding proteins[19,20]. In addition to snoRNAs, protein components of the snoRNP also associate with DDX21. We recovered NOP58, fibrillarin and dyskerin in DDX21 immunoprecipitation, both in the presence and absence of RNaseA (Fig. 3e). Conversely, NOP58 co-immunoprecipitated DDX21 (Extended Data Fig. 7c). Of note, DDX21 also binds XRN2, a snoRNA-processing exonuclease[21], but in an RNase-dependent manner (Extended Data Fig. 7d).

To explore whether DDX21 is required for snoRNP-mediated rRNA modifications[17], we assayed changes in 2′-*O*me levels using site-directed cleavage of rRNA by RNaseH[22] (Extended Data Fig. 7e). We treated HEK293 cells with control or *DDX21* 3′ UTR siRNAs, followed by expression of DDX21^{WT} or DDX21^{SAT}. Reintroduction of DDX21^{SAT} failed to rescue rRNA methylation levels at multiple sites, especially on the 28S rRNA, whereas DDX21^{WT} recovered the 2′-*O*me defects (Fig. 3f). We cannot exclude the possibility that the observed 2′-*O*me defects were due to the role of DDX21 in snoRNA transcription. However, changes in snoRNA binding pattern between DDX21^{SAT} and DDX21^{WT} can be readily detected in the absence of snoRNA transcriptional defects (Extended Data Figs 6f, g and 7f). Therefore, the helicase domain of DDX21 is required for proper binding to both rRNA and snoRNAs, suggesting a direct function within the snoRNP.

We next examined our iCLIP results for insights into the role of DDX21 in regulating Pol II-dependent transcription. While ultraviolet crosslinking to mRNAs suggested a potential *cis*-mechanism at DDX21-target genes, transcripts from most DDX21-occupied promoters were not recovered in iCLIP and only 8% of the iCLIP mRNA reads mapped within 5′ UTRs (Extended Data Fig. 8a, b). Thus, nascent RNA tethering is unlikely to be the major mechanism of DDX21 chromatin recruitment. Notably, 7SK snRNA, a well-known *trans*-acting non-coding RNA involved in Pol II transcription[23–26], was among the most highly enriched DDX21-bound RNAs (Extended Data Fig. 8c). Together with HEXIM1/2 and P-TEFb (which consists of a CDK9 and cyclin T1 heterodimer), 7SK functions to modulate Pol II promoter pause–release[27,28]. We observed DDX21 crosslinking most robustly to two specific sites on 7SK (Fig. 4a), outside the known binding sites of HEXIM1/2 and P-TEFb[29] (Extended Data Fig. 8d). Recent evidence demonstrated that the 7SK snRNP is physically associated with Pol II promoters, where P-TEFb is then released[24,25,30]. We proposed that DDX21 is recruited to Pol II promoters together with the 7SK snRNP. Consistent with this

hypothesis, protein components of the 7SK snRNP associate with DDX21 in reciprocal co-immunoprecipitation experiments (Extended Data Fig. 8e, f). Furthermore, both HEXIM1 and CDK9 are bound at DDX21-target Pol II promoters, but not at the rDNA locus (Extended Data Fig. 9a, b). Finally, depletion of 7SK with two independent antisense oligonucleotides[26] strongly reduced the association of DDX21 with Pol II-bound promoters, but not at the rDNA (Fig. 4b and Extended Data Fig. 9c), indicating that 7SK facilitates the association of DDX21 with promoters. Notably, similar to DDX21, Gene Ontology analyses of CDK9 ChIP-seq from HEK293 cells[30] revealed enrichment for components of the ribosomal pathway (Extended Data Fig. 9d), suggesting that the 7SK snRNP complex might have an inherent preference for binding at ribosomal and growth control genes. Nonetheless, this preference alone cannot entirely explain the specificity of DDX21 targeting to ribosomal genes, because we also detected HEXIM1 and CDK9 at active promoters unbound by DDX21 (Extended Data Fig. 9a, b).

Transcriptional elongation is triggered by phosphorylation of the Pol II carboxy-terminal domain at serine 2 (Ser2p) upon release of P-TEFb from 7SK[25,28,30]. To test whether DDX21 facilitates P-TEFb release, we performed a 'release assay'[24,30] by purifying the inactive form of the 7SK snRNP. Incubation of the inactive 7SK snRNP with purified Flag–HA–DDX21 resulted in the dose-dependent release of CDK9, whereas a control Flag purification showed no release (Fig. 4c, d). Consistent with its role in promoting the activity of P-TEFb, *DDX21* knockdown impaired Pol II Ser2p at the 3′ ends of DDX21-target genes (Fig. 4e). Total levels of Pol II at the same regions were also diminished, concordant with an elongation defect (Extended Data Fig. 9e).

DDX21 promotes transcription in a manner dependent on its catalytic domain (Fig. 1j and Extended Data Fig. 2d) and we proposed that this feature would extend to its role in P-TEFb release. Notably, although $DDX21^{SAT}$ is recruited to Pol II promoters, binds to 7SK and interacts with P-TEFb in the lysate (Extended Data Fig. 10a–c), it shows marked differences in the 7SK ultraviolet crosslinking as compared to $DDX21^{WT}$, with accumulation at the single-stranded region upstream from the fourth stem loop, involved in P-TEFb binding and inhibition[29] (Extended Data Fig. 10c). These observations suggest that $DDX21^{SAT}$ recognizes 7SK, but is unable to remodel the RNA. Indeed, we find that both $DDX21^{SAT}$ and an additional catalytically defective mutant, $DDX21^{DEV}$ (Extended Data Fig. 2c), failed to release P-TEFb from the inactive 7SK snRNP (Fig. 4f). Therefore, DDX21 requires its active helicase domain to drive Pol II-dependent transcription through release of P-TEFb and consequently promote transcriptional elongation.

Collectively, we showed that DDX21 is incorporated into distinct snRNP complexes, 7SK snRNP and snoRNP (Extended Data Fig. 10d), to regulate transcriptional and post-transcriptional steps of ribosome biogenesis. Our data suggest that DDX21 is a key component in coordinating transcriptional programs across distinct nuclear compartments, as its engagement with chromatin is sensitive to the status of both Pol I and Pol II. We propose that through its multifaceted function in ribosome biogenesis, DDX21 has a key role in regulating cellular growth in health and malignancy.

Online Content Methods, along with any additional Extended Data display items and Source Data, are available in the online version of the paper; references unique to these sections appear only in the online paper.

METHODS

HEK293 cells were cultured in DMEM plus 10% FBS and maintained under standard tissue culture conditions. ChIP-seq and ChIP-qPCR analyses were conducted in HEK293 cells with commercially available antibodies as described. The nascent transcript assays have been described elsewhere[31]. In brief, HEK293 cells stably expressing inducible transgenes for either DDX21^{WT} or DDX21^{SAT} were cultured in tetracycline-free serum (GIBCO) and seeded at a density of 30–50% confluency overnight. Cells were transfected for two consecutive days with a pool of siRNA targeting the *DDX21* 3′ UTR (see later in the text). Twelve hours after the second transfection, 0.025 μg ml^{-1} doxycycline (dox) was added to the media for an additional 24 h. At this point cells were treated for 1 h with either DMSO or flavopiridol (1.0 μg ml^{-1}) to inhibit Pol II elongation. For 'wash-off' cultures, cells were washed 3–4 times with pre-warmed media and allowed to recover transcription for either 30 or 60 min. Cells were immediately collected in TRIzol and RNA was extracted as described later. For immunofluorescence studies cells were fixed in methanol and stained for the indicated antibodies. Small molecule treatments with DMSO, actinomycin-D, flavopiridol or CX-5461 were done for 1 h, unless otherwise specified. iCLIP was performed from HEK293 cells stably expressing Flag–HA–DDX21. The RNaseH cleavage assay was optimized from a previously reported method to cleave RNA at specific bases in a manner sensitive to the 2′-*O*me status of the nucleotide of interest[22]. For the P-TEFb release assay, the inactive 7SK snRNP complex was purified by immobilizing HEXIM1, followed by incubation with biochemically purified Flag–HA–DDX21. The predicted 7SK structure has been published elsewhere[32].

Cell lines

HEK293 and HeLa cells were obtained from ATCC and grown under standard conditions in DMEM plus 10% FBS supplemented with antibiotics. All cell lines used in this study are mycoplasma-free. For generating stable HEK293 cells expressing Flag–HA–DDX21 (FH–DDX21) full-length *DDX21*was amplified from complementary DNA and cloned into a dox-inducible pTrip-Flag-HA lentiviral vector. The cloning strategy for generating DDX21^{DEV} and DDX21^{SAT} has been previously described[12]. HEK293 cells were infected and several clones were expanded for further analyses and tested for mycoplasma. For the iCLIP experiments, expression of the *DDX21* transgenes was achieved by addition of dox (0.025 μg ml^{-1}) to the media. Cells were collected 24 h after the addition of dox.

ChIP-qPCR and ChIP-seq

ChIP assays were performed as previously described[24,33]. In brief, HEK293 cells were cross-linked with 1% formaldehyde for 10 min at room temperature and quenched with glycine to a final concentration of 0.125 M for another 10 min. Chromatin was sonicated with a Bioruptor (Diagenode), cleared by centrifugation, and incubated overnight at 4 ºC with 5–7 μg of the desired antibodies: anti-DDX21 (Novus Biologicals BP100-1781 and

NBP1-83310), anti-Pol II Ser2p (Active Motif 61084), anti-Pol II (Santa Cruz Biotechnology sc-899), anti-CTCF (Cell Signaling 2899) anti-CDK9 (1:1 mix of Santa Cruz Biotechnology sc-8338 and sc-484). Immunocomplexes were immobilized with 100 μl of protein-G Dynal magnetic beads (Life Technologies) for 4 h at 4 ºC, followed by stringent washes and elution. Eluates were reverse cross-linked overnight at 65 ºC and deproteinated with proteinase K at 56 ºC for 30 min. DNA was extracted with phenol chloroform, followed by ethanol precipitation. ChIP-seq libraries were prepared according to the NEBNext protocol and sequenced using Illumina HiSeq 2500. ChIP-qPCR analyses were performed in a Light Cycler 480II machine (Roche). ChIP-qPCR signals were calculated as percentage of input. Fold induction was calculated over a negative genomic region. All primers used in qPCR analyses are shown in Supplementary Table 1. All ChIP antibodies have been previously validated unless otherwise specified.

ChIP-seq analyses

Sequences were mapped using DNAnexus software tools and analysed by QuEST and MACS2. For QuEST, ChIP-seq peaks were determined using a kernel density estimate bandwidth of 30, a ChIP candidate threshold of 20, a ChIP extension fold enrichment of 3, and a ChIP-to-background fold enrichment of 3. WIG files were generated with QuEST and used for visualization in the UCSC Genome Browser and for obtaining average signal profiles. Average ChIP-seq signal profiles around the centre of DDX21 ChIP-seq peaks were generated with the Sitepro tool, which is part of the Cistrome/Galaxy pipeline. We used the HOMER software to associate DDX21 ChIP-seq peaks to different genomic features. Functional annotation and Gene Ontology categories were obtained with GREAT[34]. For ascribing DDX21 binding to snoRNA-host genes, we generated a file containing all snoRNAs and their associated host genes and only snoRNAs residing within introns of RefSeq genes were used in this study. To avoid redundancies all entries were inspected manually in the UCSC genome browser.

All genomic data sets have been deposited under the GEO record GSE56802. Other data sets used in this study were obtained from GSM891237, GSE36620, GSM1249888, GSM1249889, GSE20598, GSM1249897 and GSE20598.

For mapping DDX21 ChIP-seq to the rDNA, we obtained the DNA consensus sequence of the 43-kb ribosomal locus NCBI (GeneBank ID: U13369.1). This 43 kb itself is unique relative to other locations in the human genome; however, as noted, it is repeated hundreds of times in each of the 5 chromosomal clusters. Using this unique 43-kb region, we used the Bowtie algorithm to map ChIP-seq reads with standard parameters used for mapping to the Hg19 human genome build. The same strategy has been employed by other groups to map transcription factors ChIP reads to the rDNA locus[7].

RNA extraction and qRT–PCR

RNA was isolated using Trizol (Life Technologies) according to the manufacturer's protocol. All RNA samples were DNase-treated with the Turbo DNA-Free kit (Ambion). cDNA was generated using SuperScript VILO (Life Technologies) according to

manufacturer instructions. qPCR analyses were performed on the Light Cycler 480II (Roche). All primers used are shown in Supplementary Table 1.

Immunofluorescence

EK293 cells were seeded into 24-well plates containing 12-mm glass coverslips and cultured for 16 h in DMEM containing 10% FBS (v/v). Cells were then treated for the indicated drugs (refer to the corresponding figure legends for drug concentration and time scale of the experiment). Cells were fixed in 4% paraformaldehyde for 10 min at room temperature, 3 × 5-min washes with PBS, followed by an ice-cold methanol fix for 2 min and 2 × 5-min washes with PBS. Cells were permeabilized in PBS containing 0.3% (v/v) Triton X-100 for 5 min, and blocked overnight at 4 ºC in PBT buffer (PBS with 1% BSA, 0.1% Triton X-100 (v/v), 0.05% sodium azide (w/v)). After blocking, coverslips were incubated in PBT with the corresponding antibody. For DDX21 (Novus Biologicals NBP1-83310) the antibody was diluted 1:200 and incubated at room temperature for 2 h. For fibrillarin (Cell Signaling C13C3) the antibody dilution was 1:100 and incubated at room temperature for 2 h. Coverslips had 3 × 5-min washes with PBT and incubated with the Alexa-Fluor 568 secondary antibody (1:1,000; Life Technologies) for 1 h. Cells were washed 3 × 5 min with PBT, 2 × 5 min with PBS, rinsed briefly with water and mounted onto glass slides using VECTASHIELD mounting medium with DAPI. All images were taken and processed using a Zeiss LSM700 confocal microscope.

Western blots and co-immunoprecipitation

HEK293 nuclear extracts were prepared as described previously[35]. For immunoprecipitations, extracts were incubated overnight with 3 μg of the desired antibody pre-bound to protein G-sepharose (Pierce). In some case protein extracts were treated with RNaseA (20 μg ml^{-1}). Immunocomplexes were eluted in 2× Laemmli buffer and resolved in an 8% acrylamide gel. For western blots the following antibodies were used according to manufacturer instructions: anti-NOP58 (Bethyl A302-718A); anti-fibrillarin (Cell Signaling C13C3); anti-DKC1 (Gene Tex GTX109000); anti-Flag (Sigma); anti-DDX21 (Novus Biologicals NB100-1781); anti-LARP7 (a gift from D. H. Price); anti-CDK9 (Santa Cruz Biotechnology sc-484); anti-cyclinT1 (Santa Cruz Biotechnology sc-10750); and anti-HEXIM1 (Bethyl A303-113A). All antibodies have been previously validated unless otherwise specified.

iCLIP and data analysis

The iCLIP method was performed as described before with the specific modifications below[15,36]. Twenty-four hours after dox treatment (0.025 μg ml^{-1}), FH–$DDX21^{WT}$ or FH–$DDX21^{SAT}$ HEK293 cell lines were ultraviolet crosslinked to a total of 0.3 J cm^{-2}. Whole-cell lysates were generated in CLIP lysis buffer (50 mM HEPES, 200 mM NaCl, 1 mM EDTA, 10% glycerol, 0.1% NP-40, 0.2% Triton X-100, 0.5% *N*-lauroylsarcosine) and briefly sonicated using a probe-tip Branson sonicator to solubilize chromatin. Each iCLIP experiment was normalized for total protein amount, typically 2 mg, and partially digested with RNaseA (Affymetrix) for 10 min at 37 ºC and quenched on ice. FH–DDX21 was isolated with anti-Flag agarose beads (Sigma) for 3 h at 4 ºC on rotation. Samples were washed sequentially in 1 ml for 5 min each at 4 ºC: 2 ×high stringency buffer (15 mM Tris-

HCl, pH 7.5, 5 mM EDTA, 2.5 mM EGTA, 1% Triton X-100, 1% sodium deoxycholate, 120 mM NaCl, 25 mM KCl), 1× high salt buffer (15 mM Tris-HCl pH 7.5, 5 mM EDTA, 2.5 mM EGTA, 1% Triton X-100, 1% sodium deoxycholate, 1 M NaCl), 1× NT2 buffer (50 mM Tris-HCl, pH 7.5, 150 mM NaCl, 1 mM $MgCl_2$, 0.05% NP-40). Purified FH–DDX21 was then eluted off anti-Flag agarose beads using competitive Flag peptide elution. Each sample was resuspended in 500 μl of Flag elution buffer (50 mM Tris-HCl, pH 7.5, 250 mM NaCl, 0.5% NP-40, 0.1% sodium deoxycholate, 0.5 mg ml^{-1} Flag peptide) and rotated at 4 ºC for 30 min. The Flag elution was repeated once for a total of 1 ml elution. FH–DDX21 was then captured using anti-haemagglutinin agarose beads (Pierce) for 1 h at 4 ºC on rotation. Samples were then washed as previously in the anti-Flag agarose beads. 3′-end RNA dephosphorylation, 3′-end single-stranded RNA ligation, 5′labelling, SDS–PAGE separation and transfer, autoradiograph, ribonucleoprotein isolation, proteinase K treatment, and overnight RNA precipitation took place as previously described[15]. The 3′-end single-stranded RNA ligation adaptor was modified to contain a 3′ biotin moiety as a blocking agent (Supplementary Table 1). The iCLIP library preparation was performed as described elsewhere (R.A.F., L.M., R.C.S. and H.Y.C., unpublished observations). Final library material was quantified on the BioAnalyzer High Sensitivity DNA chip (Agilent) and then sent for deep sequencing on the Illumina NextSeq machine for 1 × 75-bp cycle run. iCLIP data analysis was performed as previously described[15]. For analysis of repetitive non-coding RNAs, custom annotation files were built from the Rfam database and reads were mapped under standard iCLIP processing steps. For the repetitive RNA analysis we normalized the iCLIP reverse transcription stops across each RNA transcript, which allows the comparison of the shape of the profile, with this normalization, the *y* axis is informative only for the relative binding preference and does not imply the strength of binding.

siRNA and antisense oligonucleotide knockdown

For *DDX21* knockdown, HEK293 cells (2.5×10^5) were transfected in DMEM supplemented with 5% FBS without antibiotics using RNAiMAX (Life Technologies). *DDX21* (20 nM) or control siRNA was used in this study. Notably, DDX21 depletion was difficult to achieve, thus for efficient DDX21 knockdown (60–80% at the protein level) three consecutive siRNA transfections were required. siRNA diced pools were generated in J.W.'s laboratory using recombinant *Giardia lamblia* Dicer.

ASO depletion of 7SK was performed as previously described[26]. In brief, HEK293 cells (2×10^6) were nucleofected with the Amaxa Nucleofector 2b (Lonza) with 1 nmol of scramble control, 5′-7SK, or 3′-7SK (ref. 26). Cells were cultured for 12 h at 37 ºC and collected for ChIP-qPCR as described above. A fraction of each sample was collected with Trizol for assaying 7SK knockdown by qRT–PCR as described above.

Site-directed RNaseH rRNA cleavage assay

HEK293 cells were seeded and transfected with DDX21 or control siRNA as described above. Twelve hours after the second siRNA transfection, $DDX21^{WT}$ or $DDX21^{SAT}$ cDNAs were induced by adding 0.25 μg ml^{-1} dox, after which cells were collected by scrapping the monolayer in ice-cold PBS. Total cellular RNA was isolated by Trizol extraction and RNeasy column clean up. To evaluate the fraction of methylation of specific nucleotides

within the rRNA quantitatively, we optimized an established assay using RNaseH to cleave unmethylated RNA selectively [22]. Several sites were selected based on iCLIP reverse transcription stops to both the rRNA region of interest as well as reverse transcription stops on the targeting snoRNA transcript. Chimaeric 2′-*O*me/DNA oligonucleotides were ordered for three sites (Supplementary Table 1) each containing three DNA nucleobases for RNaseH targeting. For each cleavage reaction 1 μg of total RNA was mixed with 0.5 pmol of a specific chimaeric oligonucleotide (final volume of 6 μl) and annealed to the rRNA by incubating at 80 ºC for 2 min and then step-cooling the sample to 25 ºC, decreasing the temperature 1 ºC per second. Then 2.5 μl of 4 × RNaseH cleavage buffer (80 mM Tris-HCl, pH 7.5, 40 mM $MgCl_2$, 400 mM KCl, 0.4 mM dithiothreitol, 20 mM sucrose), 1 μl of RNaseH (Roche, note: RNaseH from this supplier is critical as other suppliers or isolates have different specificity for site-directed cleavage), and 1 μl of SUPERaseIn (Life Technologies) were added to each reaction and incubated for 25 min at 37 ºC. Samples were subsequently purified using RNeasy columns and eluted in 100 μl of water. For visualization and quantification, 5 μl of each sample was mixed with 5 μl of GLBII (Life Technologies) and heated to 65 ºC before agarose gel electrophoresis. Full-length and cleavage products were imaged and quantified on a ChemiDoc XRS + (BioRad).

P-TEFb release assay

The P-TEFb release assay was performed as previously described[37] with some modifications. Five micrograms of anti-HEXIM1 (ab25388) antibody was pre-bound to protein A Dynal magnetics beads (Life Technologies) and incubated with 2.5 mg of HeLa cell nuclear extracts to immobilize the inactive 7SK snRNP complex. The resulting immunocomplexes were incubated with increasing amounts of purified Flag–DDX21 and incubated for 2 h on ice. A magnetic separator was used to sequester the remaining HEXIM1-bound 7SK snRNP, and the resulting eluates were collected and analysed by western blotting. For purification of Flag–DDX21, nuclear extracts from HEK293 cells stably expressing Flag–DDX21 were prepared using a modified version of ref. 35. Purified nuclei were extracted in Dignam and Roeder buffer C and cleared by centrifugation. The salt concentration of the cleared extracts was adjusted to 250 mM with Dignam and Roeder buffer D. The resulting nuclear extracts were incubated with Flag–M2 aga-rose beads (Sigma) for 2 h to immobilize Flag–DDX21, followed by stringent washes: 5 × 2 min with Dignam and Roeder buffer C at an NaCl concentration of 500 mM and 1 × 5 min with buffer D-C(20 mM HEPES,20% glycerol,0.1 mM EDTA,150 mM NaCl, 0.75 mM $MgCl_2$ and 0.05 M KCl). Flag–DDX21 was eluted with the 3 × Flag peptide (Sigma) in buffer D-C.

Extended Data

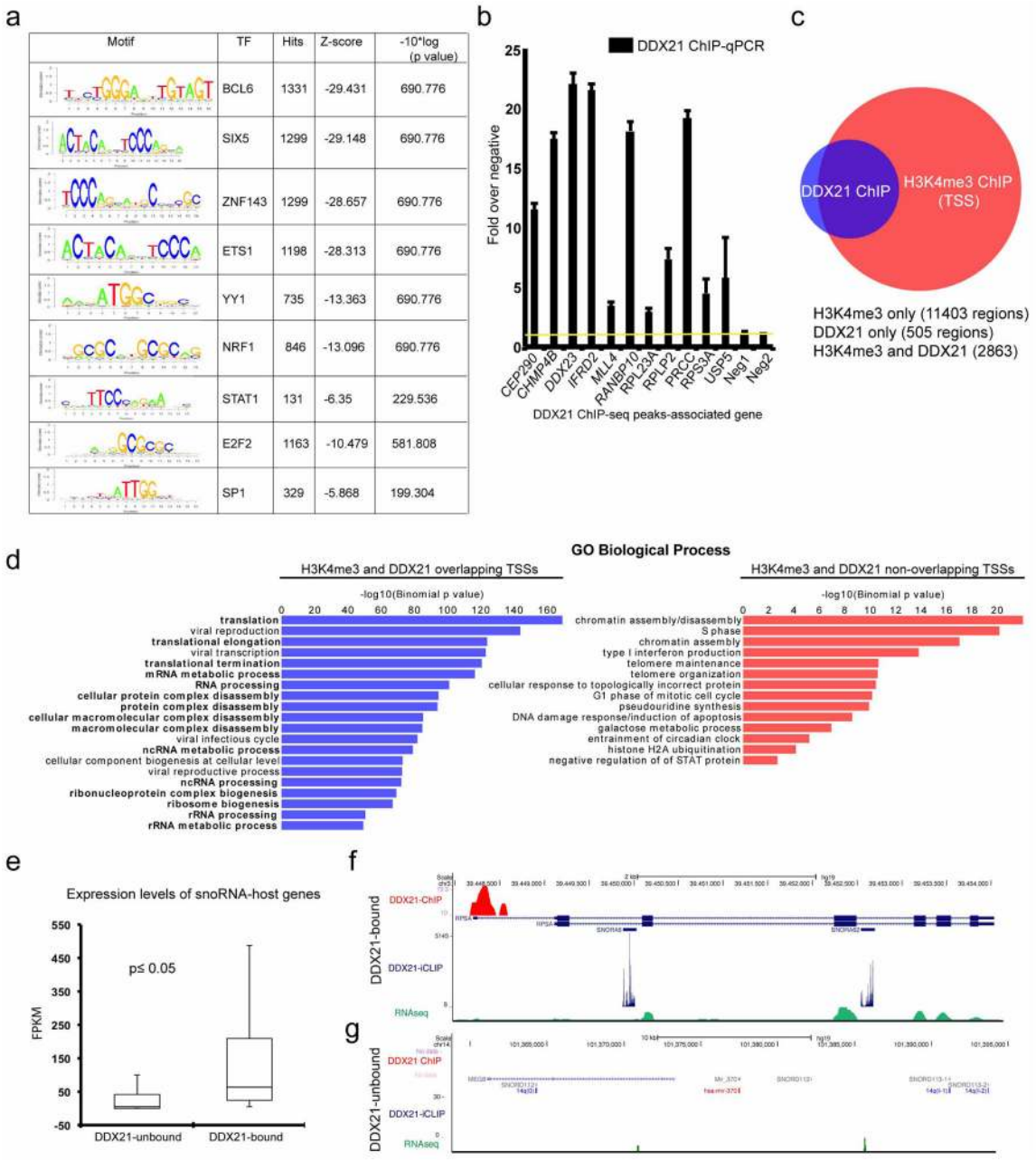

Extended Data Figure 1. DDX21 associates with non- and protein-coding ribosomal genes

a, MEME analysis of DDX21-bound regions defined by DDX21 ChIP-seq. Motif logo, annotated transcription factor, number of motif instances within the ChIP-seq regions, *Z* score, and *P* value for each motif are shown. **b**, DDX21 ChIP-qPCR from HeLa cell chromatin extracts with primers spanning a representative number of loci found to be enriched in the DDX21 ChIP-seq analyses from HEK293 cells. Data are mean and s.d. of three independent experiments. **c**, Comparison of DDX21 (this study) and H3K4me3 (publically available data, see Methods for accession numbers) ChIP-seq-bound regions.

2,863 regions are common between the data sets, 505 regions are unique to DDX21, and 11,403 regions are unique to the H3K4me3 data set. **d**, Gene Ontology terms for H3K4me3 regions that are either DDX21-bound (left) or not bound by DDX21 (right). **e**, Box plots representing the expression levels of snoRNA-host genes whose promoter regions are either bound or not by DDX21. As shown, snoRNA-host gene promoters bound by DDX21 are, on average, more highly expressed than those not occupied by DDX21. Fragments per kilobase of exon per million mapped reads (FPKM) values were taken from publically available HEK293 RNA-seq data (see Methods for accession number). The *P* value ($P \leq 0.05$) was calculated using the Wilcoxon signed-rank test. **f**, **g**, UCSC genome browser tracks depicting DDX21 ChIP-seq and iCLIP-seq, and RNA-seq enrichment profiles at differentially expressed snoRNA-host genes in HEK293 cells.

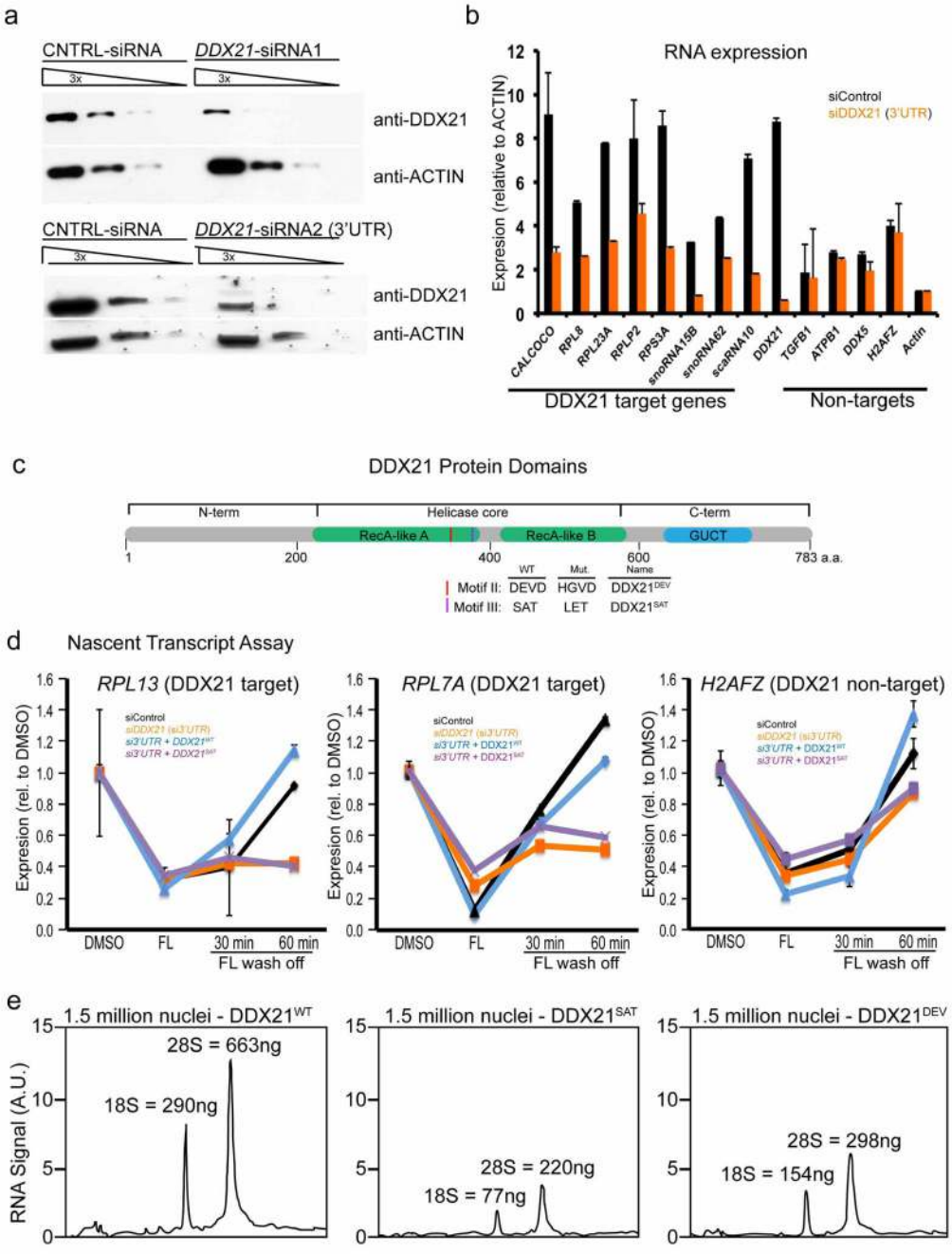

Extended Data Figure 2. DDX21 positively regulates transcription of Pol I-and Pol II-dependent ribosomal genes

a, siRNA-mediated knockdown of the DDX21 antibody used for ChIP. We transfected HEK293 cells with two different sets of siRNAs targeting endogenous *DDX21* mRNA (siRNA1 and siRNA2 (3′ UTR)) and performed western blots with the indicated antibodies. As shown, the DDX21-specific band is diminished in cells transfected with *DDX21*-targeting siRNAs, but not with control siRNAs. Actin was used as a loading control for this experiment. **b**, RT–qPCR analysis assessing the RNA expression levels of the same genes analysed in Fig. 1h upon *DDX21* knockdown by a second siRNA that targets the 3′ UTR of

DDX21 mRNA. Data are mean and s.d. of three independent experiments. For DDX21-target genes the difference between control and *DDX21* siRNA is significant, P ≤0.05 (Student's t-test). **c**, Diagram of DDX21 protein domains. The two conserved RecA-like (A and B) domains and the GUCT domains are shown in green and blue, respectively. Amino acids targeted for mutation[12] to convert DDX21^{WT} into DDX21^{SAT}, the ATP-hydrolysis mutant, are indicated with red and purple lines in the diagram. Specific amino acid changes are displayed below. **d**, qRT–PCR analysis assessing nascent unspliced mRNA levels from additional DDX21-target and DDX21-non-target promoters. For a detailed description see Fig. 1j. Data are mean and s.d. of three biological replicates. **e**, Nuclear rRNA abundance analysis by RNA BioAnalyzer of HEK293 cells depleted of DDX21 and rescued with DDX21^{WT}, DDX21^{SAT}, or DDX21^{DEV}. For each analysis, total RNA was isolated from 1,500,000 nuclei. Total nanogram amounts are shown for each of the two large rRNA subunits.

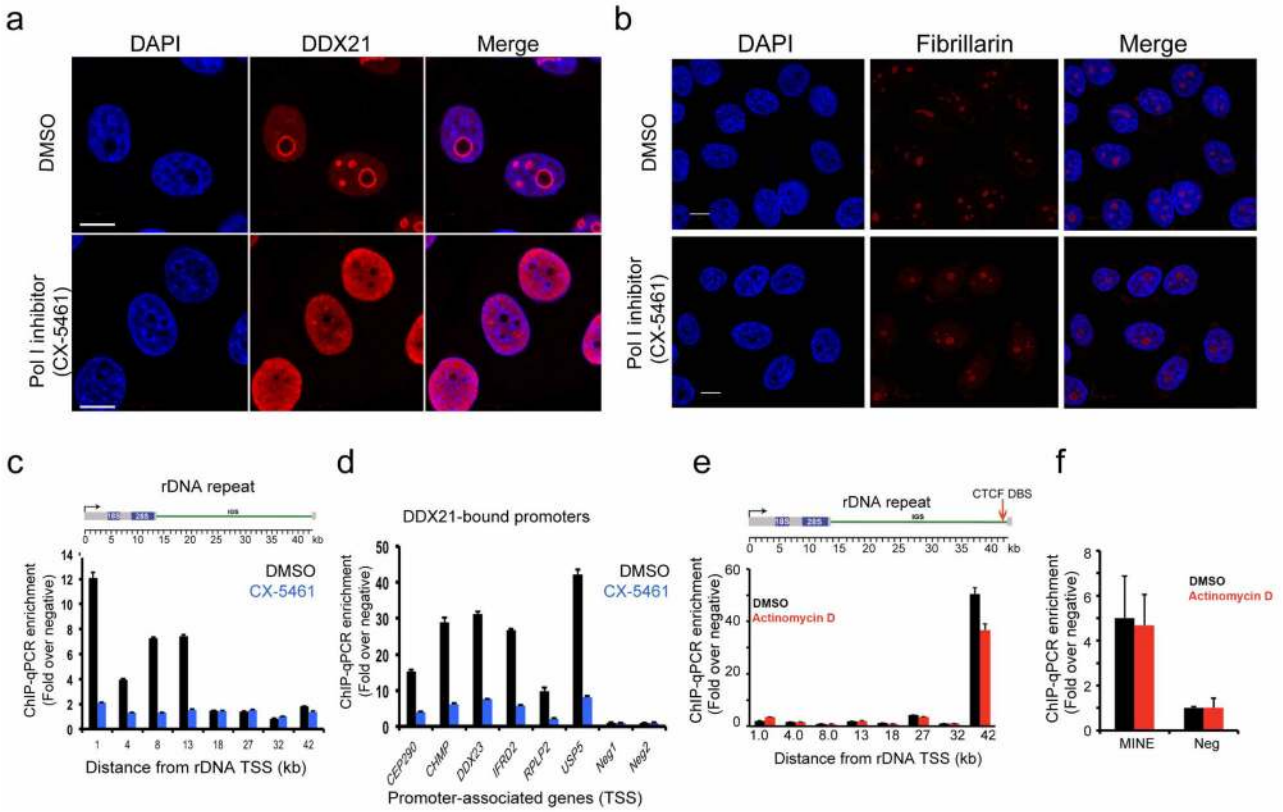

Extended Data Figure 3. Selective inhibition of Pol I alters DDX21 nuclear localization and chromatin association

a, **b**, Immunofluorescence images of methanol-fixed HEK293 cells after 1 h incubation with either DMSO or 2 μM of the specific Pol I inhibitor CX-5461. DDX21 (**a**) and fibrillarin (**b**) immuno-labellings are shown. Scale bars, 10 μm. **c**, **d**, ChIP-qPCR analyses from HEK293 sampling DDX21 genomic occupancy, at the rDNA locus (**c**) and at a representative panel of Pol II-regulated gene promoters (**d**), after treatment with DMSO or CX-5461. Data are mean and s.d. of three independent experiments. As displayed, inhibition of Pol I alters DDX21

nuclear localization and this coincides with nearly complete eviction of DDX21 from Pol I- and Pol II-regulated genes. **e**, **f**, ChIP-qPCR analyses from HEK293 cells treated with 50 ng ml^{-1} of actinomycin-D for 1 h. Binding of the transcriptional repressor CTCF across the rDNA locus (**e**) and the c-MYC insulator element (MINE) (**f**) demonstrates that actinomycin-D treatment does not effect CTCF binding to chromatin. Red arrow indicates relative location of the CTCF DNA-binding site (DBS) at the rDNA locus. Data are mean and s.d. of three independent experiments.

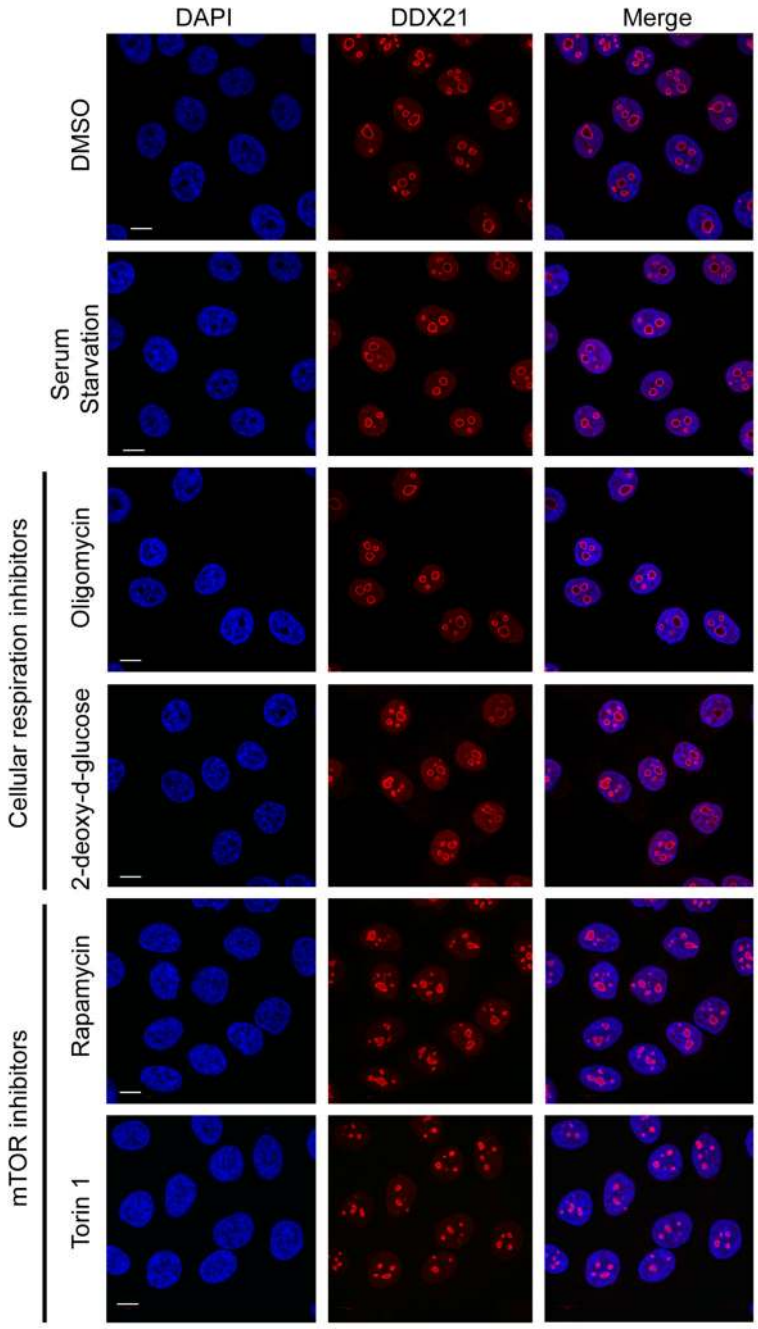

Extended Data Figure 4. DDX21 nuclear re-localization is preferentially sensitive to acute transcriptional inhibition over other cellular stressors

Immunofluorescence analyses of HEK293 cells after targeting different metabolic pathways. For inhibition of mitogen, cells were starved for 16 h in the absence of serum. For cellular respiration inhibition, cells were treated for with either oligomycin (100 μM) or 2-deoxy-D-glucose (10 mM) for 1 h. To inhibit the mTOR pathway, cells were treated with 250 nM of either Torin 1 or rapamycin for 2 h.

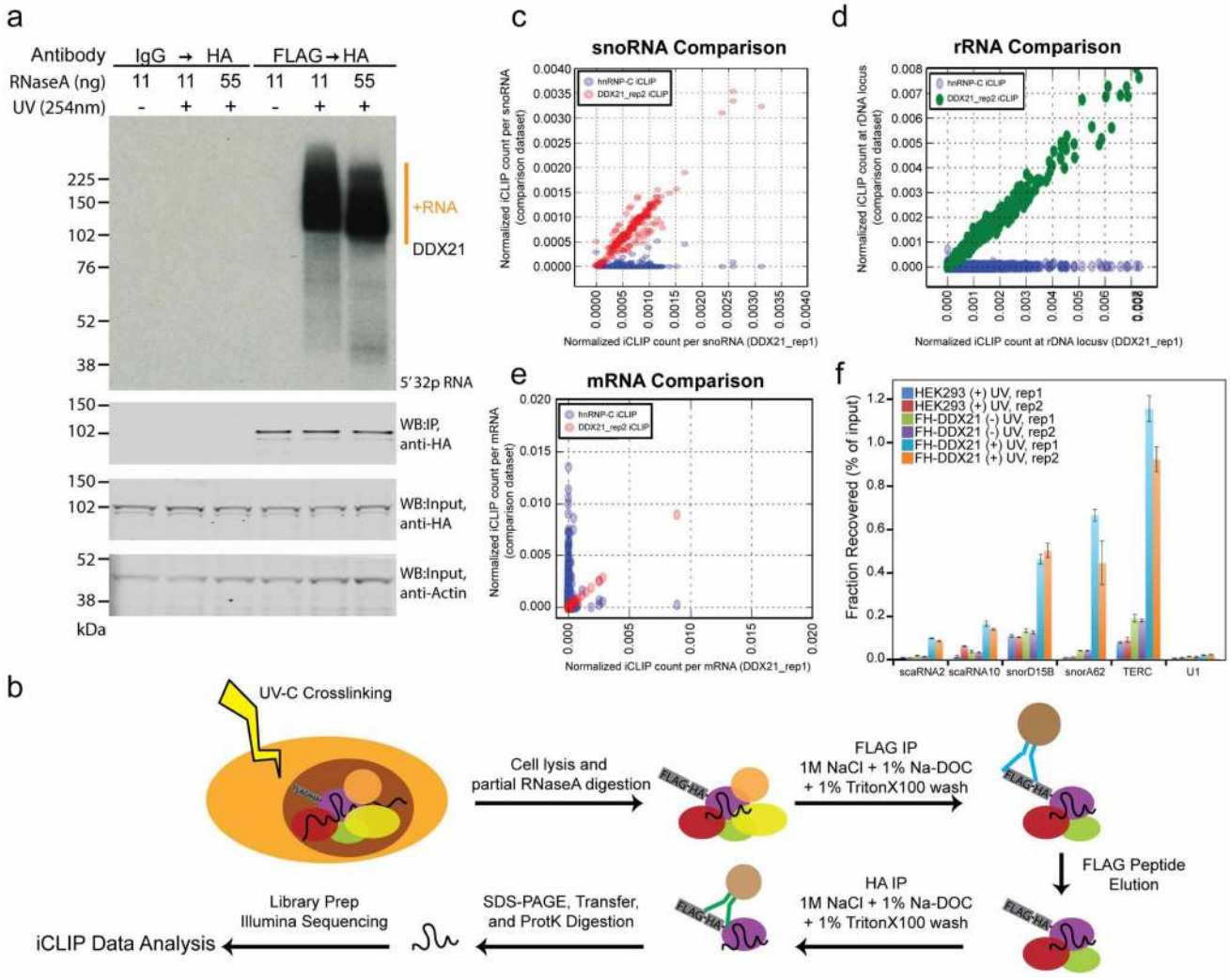

Extended Data Figure 5. Tandem affinity iCLIP of FH–DDX21^{WT}

a, FH–DDX21^{WT} iCLIP ^{32}P-autoradiogram and western blots. All samples were loaded with constant input lysate amounts (actin loading). FH–DDX21^{WT} was isolated from HEK293 cells induced to express the transgene for 24 h and crosslinked with ultraviolet light (top panel same as Fig. 3a). **b**, Schematic of the modified iCLIP procedure. To achieve high stringency and specificity Flag–HA–DDX21^{WT} is first purified on anti-Flag–M2 agarose beads, washed with 1 M NaCl, 1% Triton X-100 and 1% sodium deoxycholate. Complexes are specifically eluted with Flag peptide and recaptured with anti-HA agarose.

Standard iCLIP steps were performed thereafter to generate deep sequencing libraries. **c**–**e**, Scatter plot analysis of iCLIP reverse transcription stops on snoRNAs, rRNA and mRNAs within the FH–DDX21^{WT} (this study) and hnRNP-C (ref. 16; publically available data) data sets. Little concordance between the data sets is evident, suggesting specific transcriptome targets of these two RNA binding proteins (RBPs). **f**, DDX21^{WT} ultraviolet RNA immunoprecipitation qRT–PCR of FH–DDX21^{WT} was performed in three conditions: native HEK293 cells crosslinked with ultraviolet light; FH–DDX21^{WT} HEK293 cells without crosslinking; and FH–DDX21^{WT} HEK293 cells with ultraviolet crosslinking. snoRNAs, scaRNAs and TERC were validated targets identified in the sequencing data. Each experiment was performed in biological duplicates (rep1 and rep2) and error bars represent s.d. of technical triplicates.

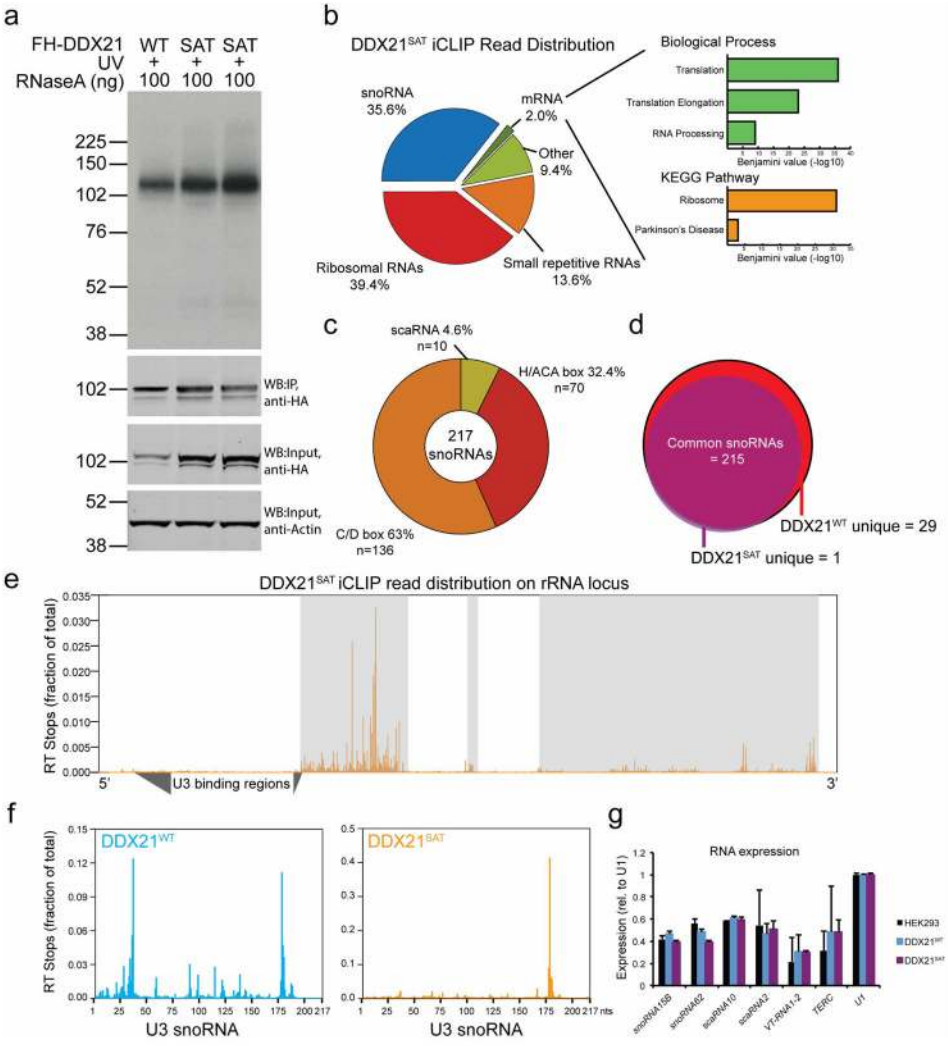

Extended Data Figure 6. Tandem affinity iCLIP of FH–DDX21^{SAT}

a, FH–DDX21^{SAT} was isolated from HEK293 cells induced to express the transgene for 24 h, at which point we did not observe significant dominant negative effects. iCLIP was performed as described for FH–DDX21^{WT}, and biological duplicates of FH–DDX21^{SAT}

iCLIP ^{32}P-autoradiogram and western blots (lanes 2 and 3) are shown. All samples were loaded with constant input lysate amounts (actin loading). FH–DDX21^{WT} was loaded as a control. WB, western blot. **b**, Left, DDX21^{SAT} iCLIP reads annotated to known repetitive (rRNA and snRNAs) and non-repetitive (hg19 genome build: mRNAs and snoRNAs) regions of the human genome. Categories are notes with their respective percentage of the total iCLIP experiment. Right, enriched Gene Ontology and KEGG pathway terms from DDX21^{SAT}-bound mRNAs obtained using the DAVID tool. The *x* axis values (in log scale) correspond to the negative Benjamini *P* value. **c**, Distribution of all DDX21^{SAT}-bound snoRNAs, representing C/D box, H/ACA box and scaRNAs. The number (*n*) and fraction (per cent) of each snoRNA type is displayed. **d**, Comparison of the snoRNAs bound by DDX21^{WT} and DDX21^{SAT}, revealing significant overlap between the active and catalytically inactive DDX21. **e**, DDX21^{SAT} iCLIP reads mapped to the transcribed region of the rDNA. **f**, DDX21^{WT} (left) and DDX21^{SAT} (right) iCLIP reads mapped to the repetitive U3 snoRNA. Binding is represented as reverse transcription stops per nucleotide normalized to the total number of reverse transcription stops mapping to the U3 snoRNA. Two strong binding sites are evident between bases 25–40 and 175–185 of U3 in DDX21^{WT} iCLIP, whereas the 5′ binding site is reduced in DDX21^{SAT}. nts, nucleotides. **g**, qRT–PCR analysis assessing the expression levels of several snoRNAs 24 h after expression of either DDX21^{WT} or DDX21^{SAT}. This experiment was performed in biological duplicates. Data are mean and s.d. of technical triplicates.

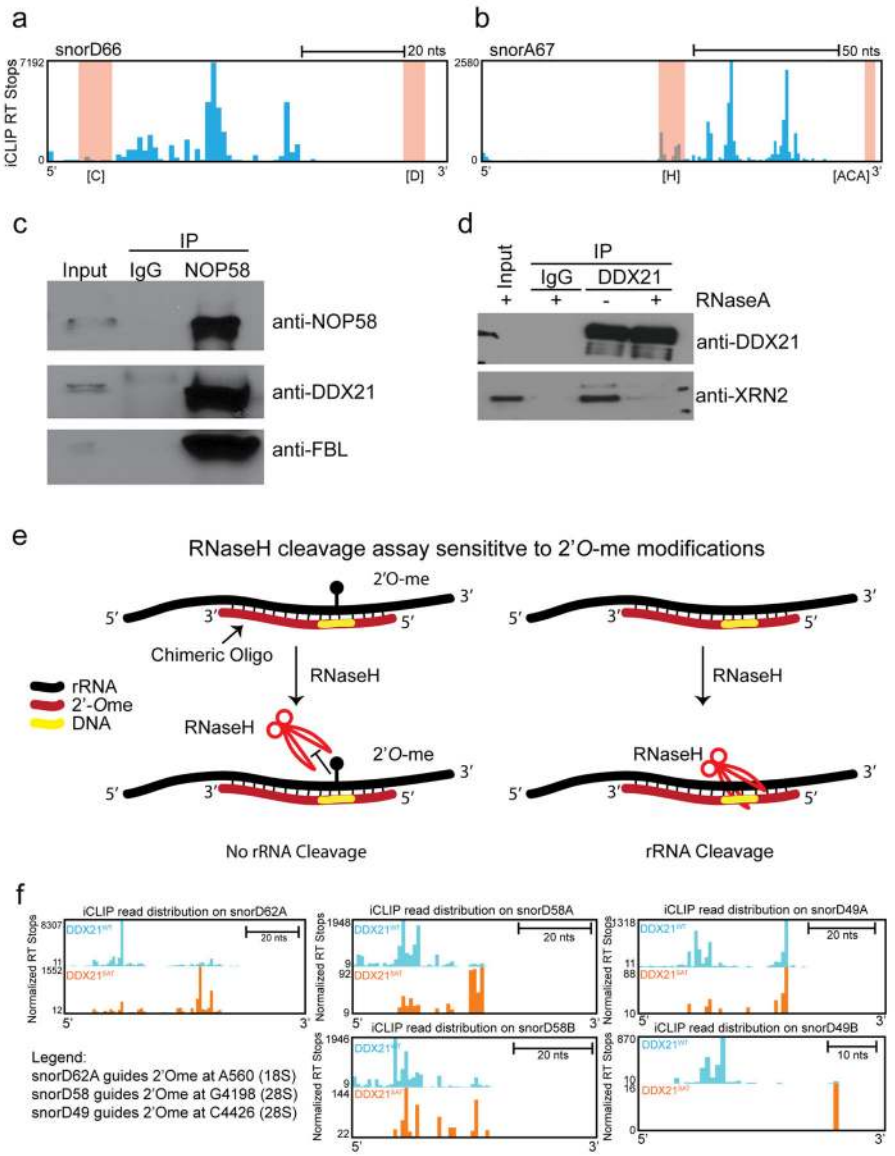

Extended Data Figure 7. DDX21 functionally interacts with snoRNAs and the snoRNP

a, UCSC genome browser view of DDX21^{WT} iCLIP reads across the snorD66 snoRNA. The C box [C] and D box [D] regions are highlighted in red. **b**, Same visualization as in **a** but showing the snorA67 snoRNA with the H box [H] and ACA box [ACA] regions highlighted. **c**, Immunoprecipitation of NOP58 from HEK293 nuclear extracts confirms DDX21 as a protein member of the snoRNP machinery. As a control for this experiment we performed western blots against FBL, a well-known NOP58-interacting partner and an essential factor of the snoRNP machinery. **d**, DDX21 interacts with XRN2, a 5′–3′ exoribonuclease required for maturation and processing of snoRNAs. The DDX21–XRN2 interaction appears to be bridged by RNA, as treatment of the nuclear lysates with RNaseA abolishes the interaction. **e**, Schematic of the site-directed RNaseH cleavage of RNA sensitive to 2′-*O*me. RNA of interest is hybridized to a 2′-*O*me/DNA chimaeric oligonucleotide in which the DNA nucleotides specifically target the ability of RNaseH to interrogate the 2′-*O*me status of a

single nucleotide. 2′-*O*me will inhibit RNaseH and leave intact RNA, while unmethylated RNA will be cleaved. **f**, UCSC genome browser view of DDX21^{WT} and DDX21^{SAT} iCLIP reads across the snoRNAs responsible for guiding the modifications tested in Fig. 3f.

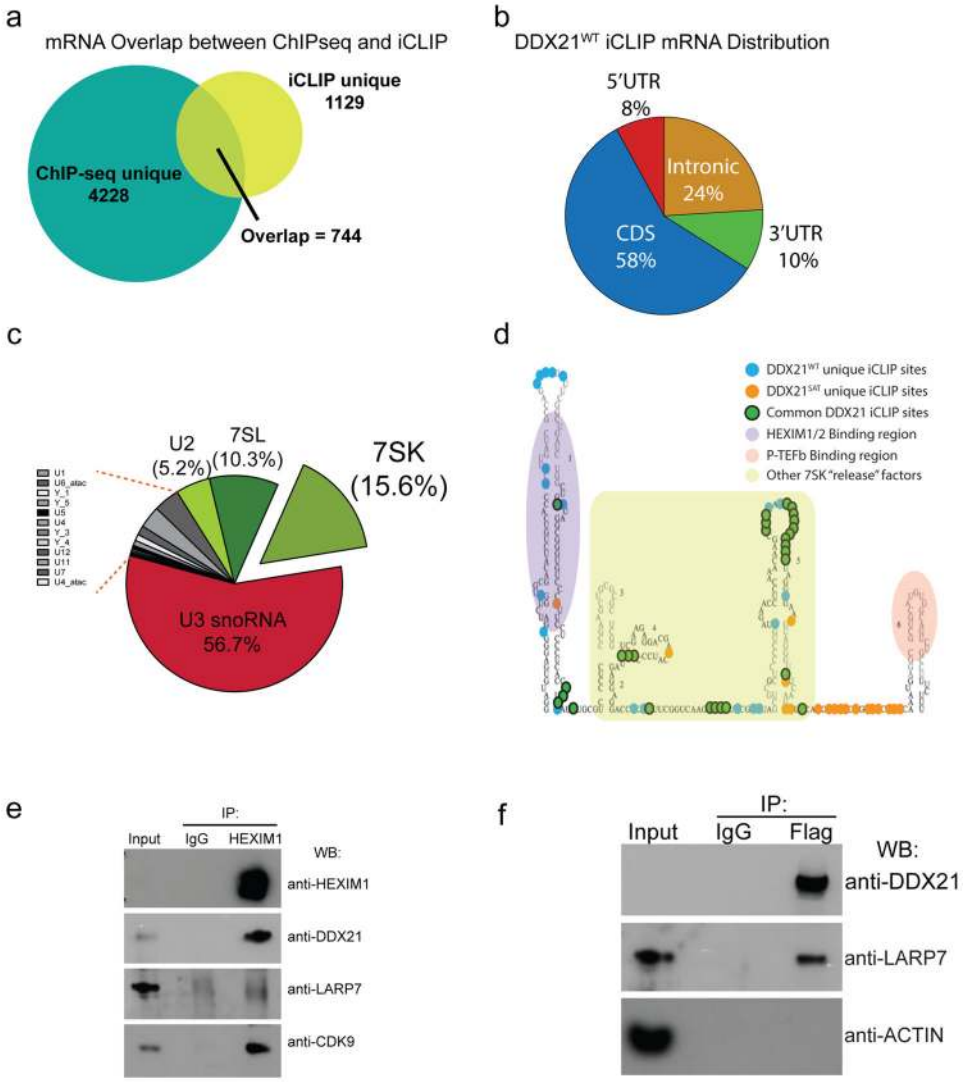

Extended Data Figure 8. Association of DDX21 with the RNA and protein components of the 7SK snRNP

a, Comparison of DDX21^{WT} ChIP-seq targets to DDX21^{WT} iCLIP-bound mRNAs. The numbers of unique and common genes are represented, revealing that most ChIP-seq-bound genes are not immunoprecipitated by iCLIP but that some are recovered in both assays. **b**, iCLIP read distribution of DDX21^{WT}-target mRNAs categorized by the regions within mRNAs that were bound. Most iCLIP reads fell outside the 5′ UTR. **c**, DDX21^{WT} iCLIP reads mapping to short repetitive RNAs of the human genome. Percentages of the top four short repetitive RNAs are shown. **d**, Secondary structure model of the 7SK snRNA annotated with iCLIP reverse transcription stops identified from the DDX21^{WT} (blue) and DDX21^{SAT} (orange) experiments. Nucleotides commonly crosslinked are labelled in green. Known RNA binding protein sites: HEXIM1/2 is highlighted in purple; P-TEFb is

highlighted in red; and other P-TEFb 'release' factors in the centre are highlighted in green. **e**, Co-immunoprecipitation analysis of HEXIM1 as assayed by western blotting for DDX21^{WT} and 7SK snRNP components (CDK9 and LARP7). **f**, Immunoprecipitation of Flag–HA–DDX21^{WT} from HEK293 nuclear extracts confirms DDX21 as a protein component of the 7SK snRNP through co-recovery of LARP7. The abundant protein actin, which is not part of the 7SK snRNP, was not recovered.

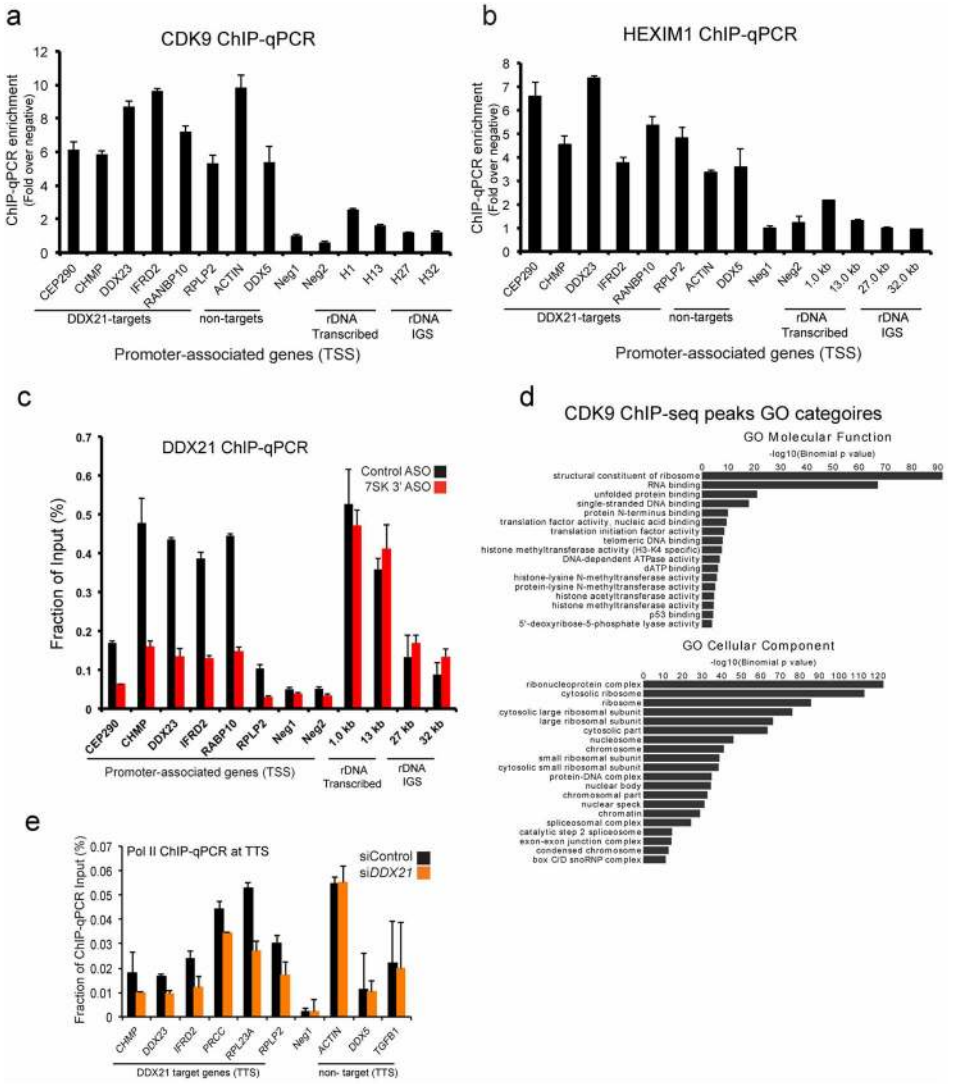

Extended Data Figure 9. Binding of the DDX21–7SK snRNP at ribosomal gene promoters

a, b, ChIP-qPCR of CDK9 (**a**) and HEXIM1 (**b**) in HEK293 cells at representative Pol II-regulated, DDX21-target and -non-target gene promoters, negative control regions, and the rDNA locus. **c**, ChIP-qPCR of DDX21 in control or 3′-7SK-ASO-treated HEK293 cells at representative Pol II-regulated, DDX21-target gene promoters, negative control regions, and the rDNA locus. For the promoter-associated genes, $P \leq 0.05$ (Student's t-test) when compared to control ASO. **d**, Gene Ontology molecular function and cellular component analysis of publically available CDK9 ChIP-seq data[30]. **e**, ChIP-qPCR of total Pol II in

control or DDX21-targeting siRNA-treated HEK293 cells at representative TSSs of Pol II-regulated, DDX21-target gene promoters and negative control regions. Data are mean and s.d. of three independent experiments.

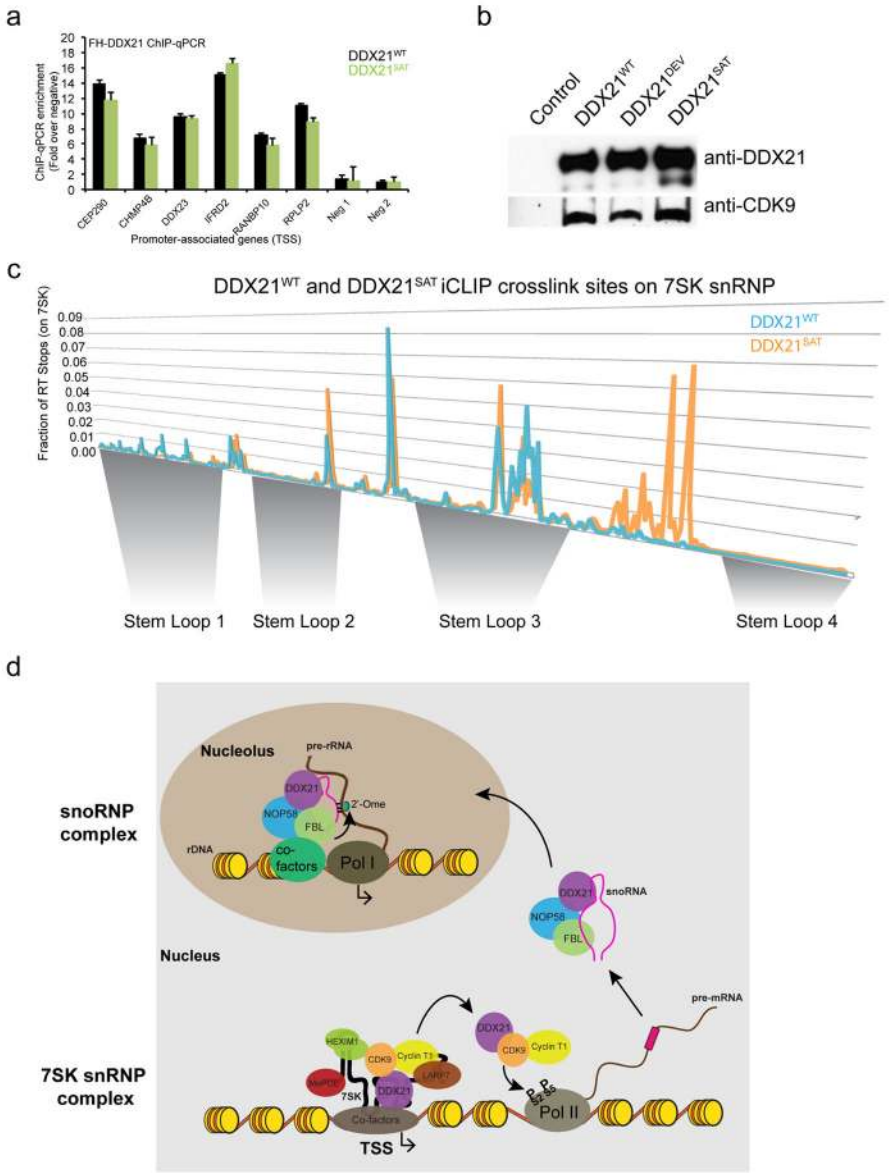

Extended Data Figure 10. Catalytically inactive DDX21 is still incorporated into the 7SK snRNP

a, ChIP-qPCR of DDX21^{WT} (black) and DDX21^{SAT} (green) in HEK293 cells at representative TSSs of Pol II-regulated, DDX21-target gene promoters and negative control regions. Data are mean and s.d. of three independent experiments. **b**, Immunoprecipitation of DDX21^{WT}, DDX21^{DEV} or DDX21^{SAT} from HEK293 nuclear extracts confirms DDX21 interacts with CDK9 (P-TEFb) regardless of its catalytic activity. **c**, DDX21^{WT} (blue) and DDX21^{SAT} (orange) annotated iCLIP reads mapped across the 7SK snRNA. The four annotated stem–loops are marked below the graph. **d**, Model of multi-level control of ribosomal pathway by DDX21. In the nucleolus, DDX21 associates with the chromatin

across the transcribed region of the rDNA and is a component of the snoRNP. Furthermore, DDX21 functionally interacts with the rRNA, snoRNAs and snoRNP to control 2′-*O*me deposition on the rRNA in a helicase activity-dependent manner. In the nucleoplasm, DDX21 is bound to the promoter regions of ribosomal Pol II-transcribed genes, many of which contain precursor snoRNA transcripts. Mechanistically, DDX21 activates transcription of its target genes through the 7SK–P-TEFb axis. As part of the 7SK snRNP, DDX21 can facilitate the release of P-TEFb from the inhibitory complex in a manner dependent on ATP hydrolysis, leading to productive Pol II elongation and increased phosphorylation of Ser 2. Efficient transcription of its target genes enforces high expression of both snoRNAs and other ribosomal proteins critical for the rRNA maturation process, placing DDX21 as a central operator of the ribosomal pathway.

Supplementary Material

Refer to Web version on PubMed Central for supplementary material.

Acknowledgments

We thank D. H. Price for the LARP7 antibody, K. Lane from M. Covert's laboratory for metabolic inhibitors, K. Cimprich and members of the Chang and Wysocka laboratories for discussions, and B. Zarnegar and P. Khavari for discussions regarding iCLIP. This work was supported by the Stanford Medical Scientist Training Program and T32CA09302 (R.A.F.), AP Giannini Foundation (R.C.S.), National Institutes of Health grants R01-HG004361, R01-ES023168, P50-HG007735 (H.Y.C.) and R01-GM095555 (J.W.), W. M. Keck Foundation (J.W.), and Helen Hay Whitney Foundation (E.C.). H.Y.C. is an Early Career Scientist of the Howard Hughes Medical Institute.

References

1. Rocak S, Linder P. DEAD-box proteins: the driving forces behind RNA metabolism. Nature Rev Mol Cell Biol. 2004; 5:232–241. [PubMed: 14991003]
2. Russell R, Jarmoskaite I, Lambowitz AM. Toward a molecular understanding of RNA remodeling by DEAD-box proteins. RNA Biol. 2013; 10:44–55. [PubMed: 22995827]
3. Putnam AA, Jankowsky E. DEAD-box helicases as integrators of RNA, nucleotide and protein binding. Biochim Biophys Acta. 2013; 1829:884–893. [PubMed: 23416748]
4. Henning D, So RB, Jin R, Lau LF, Valdez BC. Silencing of RNA helicase II/Guα inhibits mammalian ribosomal RNA production. J Biol Chem. 2003; 278:52307–52314. [PubMed: 14559904]
5. Yang H, et al. Down-regulation of RNA helicase II/Gu results in the depletion of 18 and 28 S rRNAs in *Xenopus* oocyte. J Biol Chem. 2003; 278:38847–38859. [PubMed: 12851405]
6. Westermarck J, et al. The DEXD/H-box RNA helicase RHII/Gu is a co-factor for c-Jun-activated transcription. EMBO J. 2002; 21:451–460. [PubMed: 11823437]
7. Zentner GE, Saiakhova A, Manaenkov P, Adams MD, Scacheri PC. Integrative genomic analysis of human ribosomal DNA. Nucleic Acids Res. 2011; 39:4949–4960. [PubMed: 21355038]
8. Cong R, et al. Interaction of nucleolin with ribosomal RNA genes and its role in RNA polymerase I transcription. Nucleic Acids Res. 2012; 40:9441–9454. [PubMed: 22859736]
9. Dieci G, Preti M, Montanini B. Eukaryotic snoRNAs: a paradigm for gene expression flexibility. Genomics. 2009; 94:83–88. [PubMed: 19446021]
10. Chao SH, et al. Flavopiridol inhibits P-TEFb and blocks HIV-1 replication. J Biol Chem. 2000; 275:28345–28348. [PubMed: 10906320]
11. Chao SH, Price DH. Flavopiridol inactivates P-TEFb and blocks most RNA polymerase II transcription *in vivo*. J Biol Chem. 2001; 276:31793–31799. [PubMed: 11431468]

12. Valdez BC, Henning D, Perumal K, Busch H. RNA-unwinding and RNA-folding activities of RNA helicase II/Gu–two activities in separate domains of the same protein. Eur J Biochem. 1997; 250:800–807. [PubMed: 9461305]
13. Perlaky L, Valdez BC, Busch H. Effects of cytotoxic drugs on translocation of nucleolar RNA helicase RH-II/Gu. Exp Cell Res. 1997; 235:413–420. [PubMed: 9299166]
14. Drygin D, et al. Anticancer activity of CX-3543: a direct inhibitor of rRNA biogenesis. Cancer Res. 2009; 69:7653–7661. [PubMed: 19738048]
15. Huppertz I, et al. iCLIP: Protein-RNA interactions at nucleotide resolution. Methods. 2014; 65:274–287. [PubMed: 24184352]
16. Zarnack K, et al. Direct competition between hnRNP C and U2AF65 protects the transcriptome from the exonization of Alu elements. Cell. 2013; 152:453–466. [PubMed: 23374342]
17. Lui L, Lowe T. Small nucleolar RNAs and RNA-guided post-transcriptional modification. Essays Biochem. 2013; 54:53–77. [PubMed: 23829527]
18. Hughes JM, Ares M Jr. Depletion of U3 small nucleolar RNA inhibits cleavage in the 5′ external transcribed spacer of yeast pre-ribosomal RNA and impairs formation of 18S ribosomal RNA. EMBO J. 1991; 10:4231–4239. [PubMed: 1756730]
19. Fatica A, Galardi S, Altieri F, Bozzoni I. Fibrillarin binds directly and specifically to U16 box C/D snoRNA. RNA. 2000; 6:88–95. [PubMed: 10668801]
20. Newman DR, Kuhn JF, Shanab GM, Maxwell ES. Box C/D snoRNA-associated proteins: two pairs of evolutionarily ancient proteins and possible links to replication and transcription. RNA. 2000; 6:861–879. [PubMed: 10864044]
21. Petfalski E, Dandekar T, Henry Y, Tollervey D. Processing of the precursors to small nucleolar RNAs and rRNAs requires common components. Mol Cell Biol. 1998; 18:1181–1189. [PubMed: 9488433]
22. Yu YT, Shu MD, Steitz JA. A new method for detecting sites of 2′-O-methylation in RNA molecules. RNA. 1997; 3:324–331. [PubMed: 9056769]
23. Yang Z, Zhu Q, Luo K, Zhou Q. The 7SK small nuclear RNA inhibits the CDK9/cyclin T1 kinase to control transcription. Nature. 2001; 414:317–322. [PubMed: 11713532]
24. Ji X, et al. SR proteins collaborate with 7SK and promoter-associated nascent RNA to release paused polymerase. Cell. 2013; 153:855–868. [PubMed: 23663783]
25. McNamara RP, McCann JL, Gudipaty SA, D'Orso I. Transcription factors mediate the enzymatic disassembly of promoter-bound 7SK snRNP to locally recruit P-TEFb for transcription elongation. Cell Rep. 2013; 5:1256–1268. [PubMed: 24316072]
26. Castelo-Branco G, et al. The non-coding snRNA 7SK controls transcriptional termination, poising, and bidirectionality in embryonic stem cells. Genome Biol. 2013; 14:R98. [PubMed: 24044525]
27. Nguyen VT, Kiss T, Michels AA, Bensaude O. 7SK small nuclear RNA binds to and inhibits the activity of CDK9/cyclin T complexes. Nature. 2001; 414:322–325. [PubMed: 11713533]
28. Peterlin BM, Price DH. Controlling the elongation phase of transcription with P-TEFb. Mol Cell. 2006; 23:297–305. [PubMed: 16885020]
29. Michels AA, et al. Binding of the 7SK snRNA turns the HEXIM1 protein into a P-TEFb (CDK9/cyclin T) inhibitor. EMBO J. 2004; 23:2608–2619. [PubMed: 15201869]
30. Liu W, et al. Brd4 and JMJD6-associated anti-pause enhancers in regulation of transcriptional pause release. Cell. 2013; 155:1581–1595. [PubMed: 24360279]
31. Flynn RA, Almada AE, Zamudio JR, Sharp PA. Antisense RNA polymerase II divergent transcripts are P-TEFb dependent and substrates for the RNA exosome. Proc Natl Acad Sci USA. 2011; 108:10460–10465. [PubMed: 21670248]
32. Wassarman DA, Steitz JA. Structural analyses of the 7SK ribonucleoprotein (RNP), the most abundant human small RNP of unknown function. Mol Cell Biol. 1991; 11:3432–3445. [PubMed: 1646389]
33. Sharma A, et al. The Werner syndrome helicase is a cofactor for HIV-1 long terminal repeat transactivation and retroviral replication. J Biol Chem. 2007; 282:12048–12057. [PubMed: 17317667]

34. McLean CY, et al. GREAT improves functional interpretation of cis-regulatory regions. Nature Biotechnol. 2010; 28:495–501. [PubMed: 20436461]

35. Carey MF, Peterson CL, Smale ST. Dignam and Roeder nuclear extract preparation. Cold Spring Harb Protoc. 2009; 200910.1101/pdb.prot5330

36. Konig J, et al. iCLIP–transcriptome-wide mapping of protein–RNA interactions with individual nucleotide resolution. J Vis Exp. 2011; 50:2638. [PubMed: 21559008]

37. Krueger BJ, Varzavand K, Cooper JJ, Price DH. The mechanism of release of P-TEFb and HEXIM1 from the 7SK snRNP by viral and cellular activators includes a conformational change in 7SK. PLoS ONE. 2010; 5:e12335. [PubMed: 20808803]

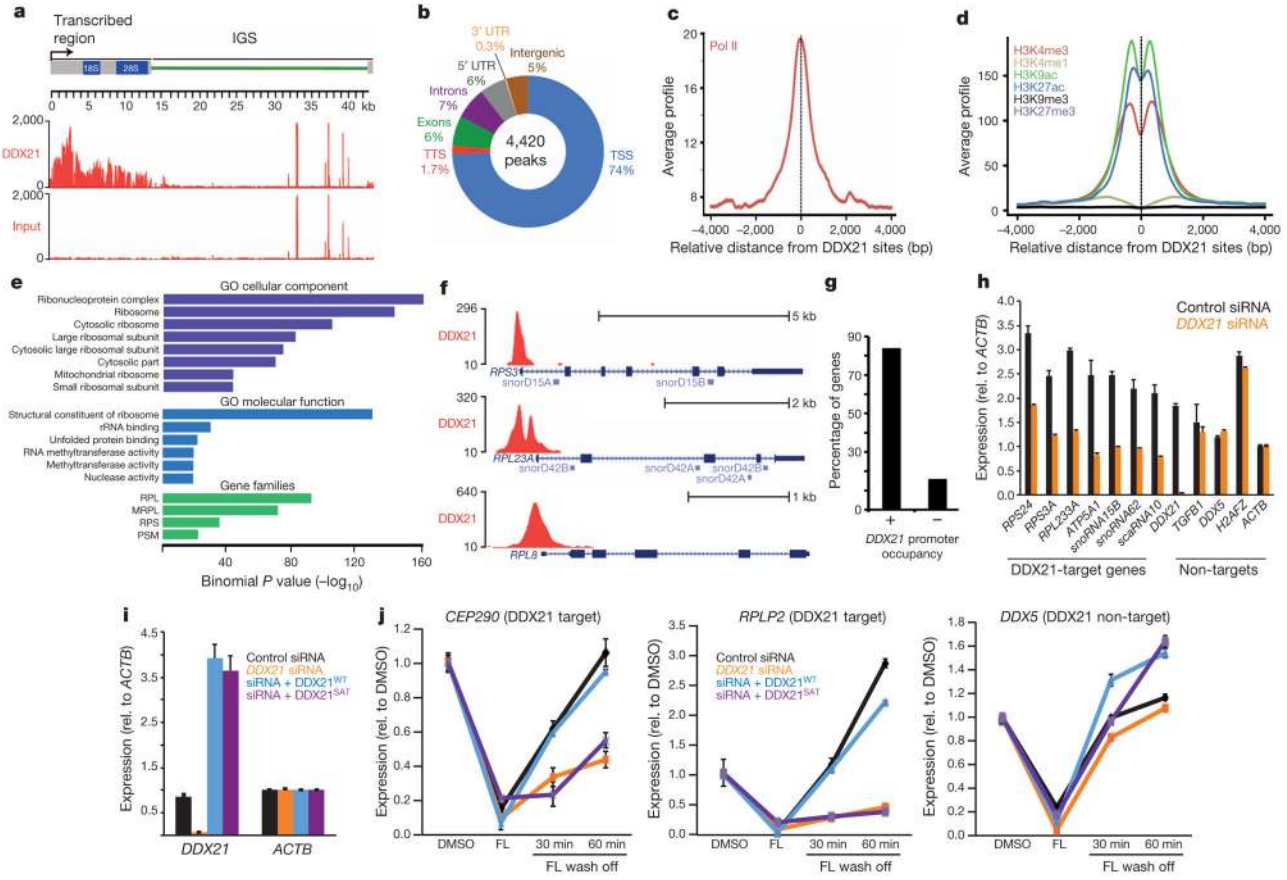

Figure 1. DDX21 associates with actively transcribed ribosomal genes

a, DDX21 ChIP-seq reads were mapped to a custom annotation file of the human rDNA locus and compared to input reads. IGS, intergenic spacer. **b**, Distribution of DDX21 ChIP-seq peaks over known genomic features. TSS, transcription start site; TTS, transcription termination site. **c**, **d**, Average ChIP-seq signal profiles from publically available data sets (see Methods) were generated for Pol II (**c**) and the indicated histone modifications around the centre of DDX21-bound regions (**d**). bp, base pairs. **e**, Genomic regions enrichment of annotations tool (GREAT) analyses of DDX21-bound regions. The *x* axis corresponds to the negative binomial *P* values. GO, Gene Ontology. **f**, University of California Santa Cruz (UCSC) genome browser tracks of DDX21 ChIP-seq at ribosomal genes containing intronic snoRNAs. **g**, Quantitative assessment of DDX21 binding to the promoters of snoRNA host genes. **h**, qRT–PCR analysis of a representative panel of DDX21-bound genes upon *DDX21* knockdown. Bars represent the average of three independent experiments. For DDX21-target genes, expression difference $P < 0.05$ (Student's *t*-test). **i**, qRT–PCR analysis of *DDX21* levels after transfecting control or *DDX21* siRNA and/or subsequent overexpression of siRNA-resistant DDX21^{WT} or DDX21^{SAT}. **j**, qRT–PCR analysis assessing the synthesis of newly made, unspliced transcripts upon *DDX21* knockdown and/or reconstitution with siRNA-resistant DDX21^{WT} or DDX21^{SAT} (see Methods). Data are mean and s.d. of three independent biological replicates. DMSO, dimethylsulphoxide; FL, flavopiridol.

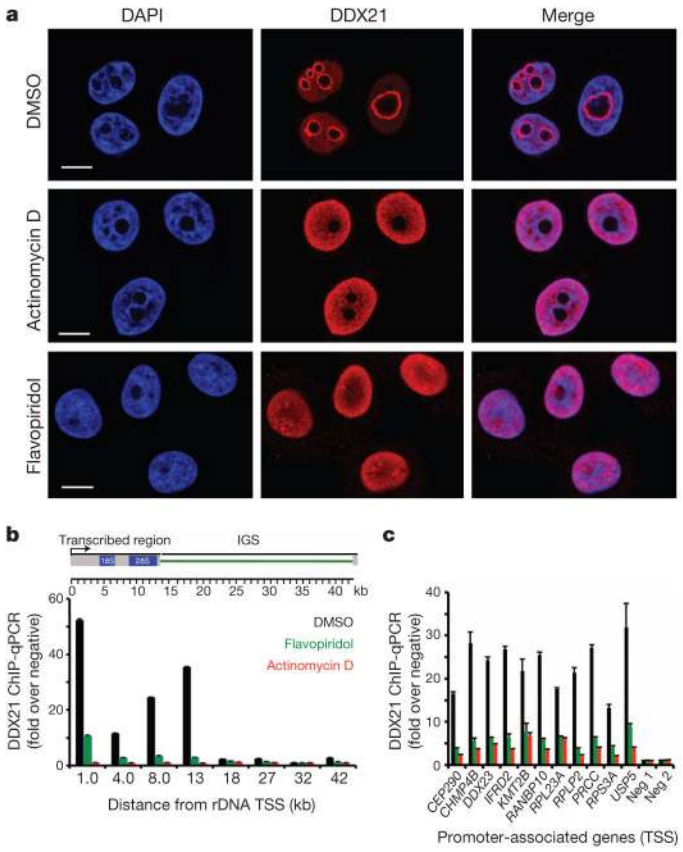

Figure 2. DDX21 chromatin association is sensitive to Pol I and Pol II transcriptional status

a, Representative immunofluorescence images of methanol-fixed HEK293 cells after 1-h incubation with DMSO, actinomycin-D (50 ng ml^{-1}) or flavopiridol (1 μM). Scale bars, 10 μm. DAPI, 4′,6-diamidino-2-phenylindole. **b**, **c**, ChIP-qPCR analysis in HEK293 cells sampling DDX21 genomic occupancy at the rDNA locus and at a representative panel of Pol II-regulated, DDX21-target promoters, upon treatment with DMSO, actinomycin-D or flavopiridol. Data are mean and s.d. of three independent experiments. Neg, negative controls.

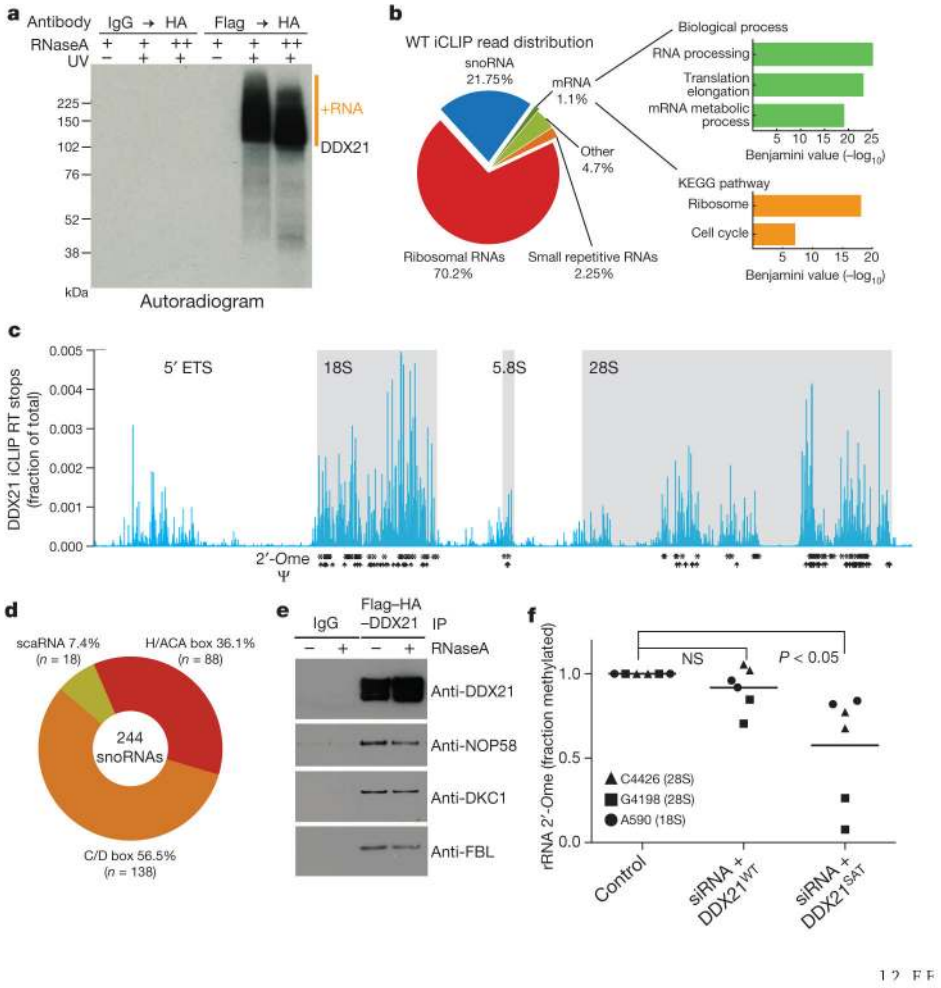

Figure 3. DDX21 binds rRNA and snoRNAs and facilitates rRNA modification

a, Autoradiogram of ^{32}P-labelled RNA crosslinked to Flag–HA–DDX21^{WT}. RNA–protein complexes are seen in the purifications from Flag–HA–DDX21^{WT} cells but not from control cells. kDa, kilodaltons; UV, ultraviolet crosslinking. **b**, Left, DDX21 iCLIP reads annotated to known repetitive (rRNA and snRNAs) and non-repetitive regions of the human genome with percentage of the total iCLIP reads shown. Right, enriched Gene Ontology and KEGG pathway terms from DDX21-bound mRNAs obtained using the DAVID tool. The *x* axis values correspond to the negative Benjamini *P* value. **c**, DDX21^{WT} iCLIP reads mapped to the transcribed region of the rDNA. The mature portions of the 18S, 5.8S and 28S rRNAs are highlighted (grey). Known 2′-*O*me (*) and Ψ (↑) modification sites are marked below the iCLIP reads. RT, reverse transcription. ETS, external transcribed spacer. **d**, Distribution of all DDX21^{WT}-bound snoRNAs, representing C/D box, H/ACA box, and scaRNAs. The number (*n*) and fraction of each snoRNA type are displayed. **e**, Co-immunoprecipitation analysis of Flag–HA–DDX21^{WT} and components of the snoRNPs. Conditions with/without RNaseA treatment are shown. **f**, Site-directed cleavage of rRNA by RNaseH at three sites. Values from three biological replicates are shown. Student's *t*-test was performed and only DDX21^{SAT} was significantly reduced ($P < 0.05$) relative to control. NS, not significant.

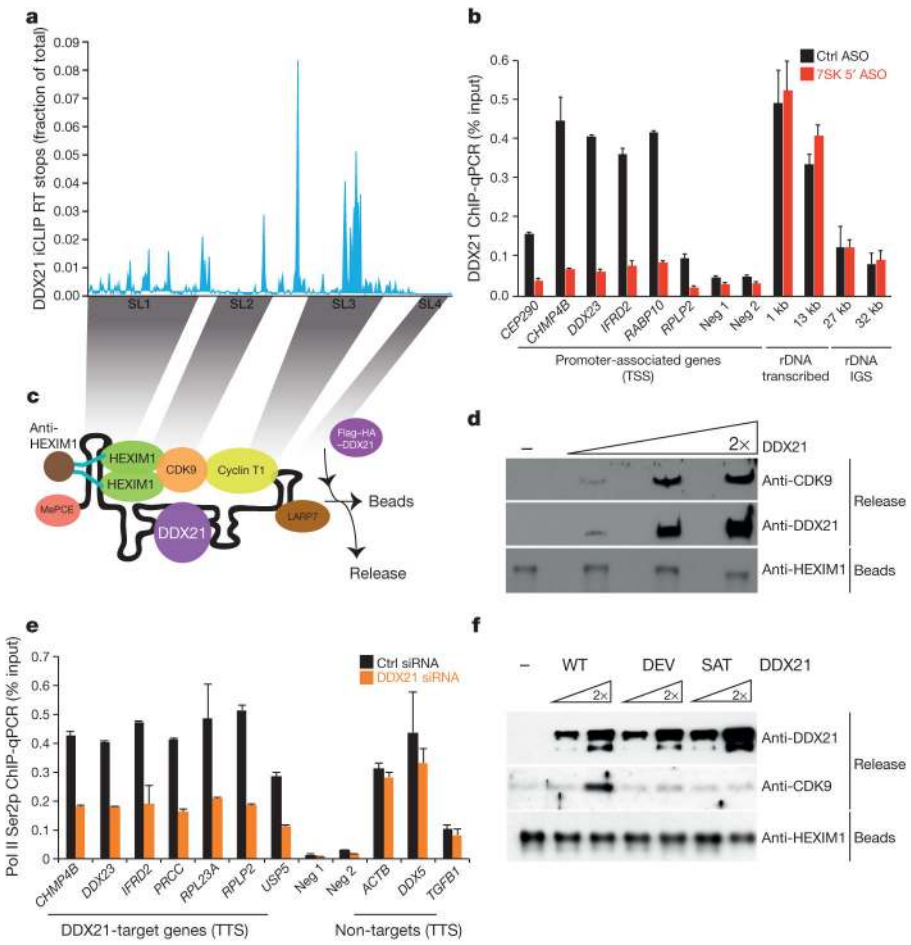

Figure 4. DDX21 promotes release of P-TEFb from the 7SK snRNP

a, DDX21^{WT} iCLIP reads mapped to the 7SK snRNA. The four stem–loops (SL1–4) are marked below the iCLIP reads and are shadowed on the cartoon in **c. b**, ChIP-qPCR of DDX21 in control or 5′-7SK-antisense oligonucleotide (ASO)-treated HEK293 cells at representative Pol II-regulated, DDX21-target gene promoters, negative control regions (Neg), and the rDNA locus. Data are mean and s.d. For DDX21-target genes the difference between control ASO and 5′ ASO is significant at $P < 0.05$ (Student's t-test). **c**, **d**, Schematic (left) and western blot analysis (right) of a P-TEFb release assay as a function of increasing amounts of DDX21^{WT}. **e**, ChIP-qPCR of Pol II Ser2p of representative Pol II-regulated genes at their transcriptional termination sites (TTS) in control or *DDX21*-siRNA-treated cells. Data are mean and s.d. of three independent experiments. **f**, Western blot analyses of a P-TEFb release assay with either DDX21^{WT} or catalytically impaired DDX21^{DEV} and DDX21^{SAT}.